UNIVERSITY OF GOTHENBURG

Citation for the published paper:

MEK inhibitor trametinib does not prevent the growth of anaplastic lymphoma kinase (ALK)–addicted neuroblastomas
Ganesh Umapathy, Jikui Guan, Dan E. Gustafsson, Niloufar Javanmardi, Diana Cervantes-Madrid, Anna Djos, Tommy Martinsson, Ruth H. Palmer, Bengt Hallberg
Sci. Signal. 28 Nov 2017:
Vol. 10, Issue 507, eaam7550
DOI: 10.1126/scisignal.aam7550

MEK inhibitor trametinib does not prevent the growth of anaplastic lymphoma kinase (ALK)-addicted neuroblastomas.

Ganesh Umapathy[1], Jikui Guan[1], Dan E. Gustafsson[1], Niloufar Javanmardi[2], Diana Cervantes-Madrid[1], Anna Djoos[2], Tommy Martinsson[2], Ruth H. Palmer[1], Bengt Hallberg[1,*].

[1]Department of Medical Biochemistry and Cell Biology, [2] Department of Clinical Pathology and Genetics, Institute of Biomedicine, Sahlgrenska academy, University of Gothenburg, SE-405 30 Göteborg, Sweden.

***Correspondence:**
Bengt Hallberg,
Department of Medical Biochemistry and Cell Biology,
Institute of Biomedicine,
Sahlgrenska Academy, University of Gothenburg,
SE-405 30 Göteborg, Sweden.
Email.bengt.hallberg@gu.se

One sentence summary: AKT/mTORC2 dependence in ALK^+ neuroblastoma cells.

Key words: Neuroblastoma, Anaplastic lymphoma kinase, PI3K, ERK5, Trametinib, mTORC2.

No conflict of interest

Abstract

The RAS-RAF-MEK-ERK pathway is a major player in initiation and progression of multiple cancers where it can be hyper-activated by upstream regulatory proteins, such as tyrosine kinases, phosphatases and GTPases. Several inhibitors targeting the RAS-MAPK pathway exhibit anti-cancer activity and are approved as single agent in specific cancers. One such is the MEK inhibitor trametinib, which is included as a rational poly therapy strategy for treating EML4-ALK, EGFR and K-RAS mutant lung cancer and neuroblastoma containing hyper-activating RAS-MAPK pathway mutations. In neuroblastoma, a heterogeneous disease, relapse cases display an increased rate of mutations of ALK, NRAS, NF1 genes, leading to hyper-activation of RAS-MAPK signaling. Targeting the RAS-MAPK pathways offers attractive options for combinatorial treatment together with ALK inhibitors, since mono-treatment has not yet produced strong clinical results in ALK-positive neuroblastoma patients. Here we investigate the response of ALK-positive neuroblastoma cell lines to MEK inhibition, employing trametinib. We show that pharmacological inhibition of the MEK-ERK pathway in ALK-positive neuroblastoma cells results in increased levels of activation/phosphorylation of AKT and ERK5. This feedback response is regulated by the mTORC2 complex protein SIN1. Taken together, our results indicate that blocking MEK-ERK leads to 'increased activation' of AKT signalling core in ALK-positive neuroblastoma, intensifying survival signals in these cells. Our results contraindicate use of MEK inhibitors as effective single and poly-therapeutic strategy in ALK-positive neuroblastoma.

Introduction

The MEK protein kinase occupies a crucial signalling node downstream of RAS and RAF and directly upstream of ERK and as such has been the subject of intensive drug discovery activities. Genetic and biochemical analyses of MEK function have suggested that MEK activity is necessary for the transforming and proliferative effects of this pathway, suggesting that therapeutics that completely inhibit MEK function may have utility in the treatment of cancers driven by activation of the RAS-RAF-MEK-MAPK axis. The mitogen-activated protein kinase (MAPK) signaling axis is involved in cancer initiation, maintenance and resistance to therapy. MAPK activation often occurs through mutations and amplifications in upstream receptor tyrosine kinases (*ALK, EGFR, ERBB2*), mutations in signal transduction genes (*NRAS, KRAS*), and/or pathway regulatory genes (*NF1, PTPN11*) (*1*) .

MEK inhibitors, such as trametinib, suppress signalling through the mitogen-activated protein kinase (MAPK) cascade displaying anti-cancer activity and are approved as a single agents for treatment of BRAF positive melanoma (*2-4*). Recently, MEK inhibitors, such as trametinib, selumetinib and binimetinib have been included as a rational polytherapy strategy for treating EML4-ALK, EGFR and K-RAS-mutant lung cancer as well as for naïve and relapsed high risk neuroblastoma containing hyper-activating RAS-MAPK mutations (*5-13*). Here we investigate the polytherapy hypothesis in ALK-positive neuroblastoma employing trametinib and ALK inhibitors. Our aim was to address whether MEK inhibition alone or in combination has therapeutic value in neuroblastoma through evaluation of a large panel of neuroblastoma cell lines.

Neuroblastoma (NB) is derived from the neural crest of the postganglionic sympathetic nervous system and is a heterogeneous disease with a span from spontaneous regression to untreatable progression. New treatment approaches, including surgery, chemoradiotherapy, stem cell transplantation, and immunotherapy, have improved cure rates but high risk neuroblastoma patients are still challenging (*14-17*). Genetically neuroblastoma is characterized by frequent deletion of parts of the chromosomes 1p and 11q, gain of parts of 17q, and/or *MYCN* gene amplification (*18-20*). The gene Anaplastic Lymphoma Kinase (ALK), a receptor tyrosine kinase (RTK) was identified as a neuroblastoma predisposition gene and constitutive active mutations were found and verified to be active within the kinase domain in both germline and in somatically acquired neuroblastoma (*21-25*). Moreover, the incidence of activating ALK point mutations in relapsed neuroblastoma patients has also been described

and is estimated to reach between 20-43% (*8, 26-28*). With this in mind, the rational for combinatorial treatment of neuroblastoma is well grounded hypothesis since previously preclinical combinations of tyrosine kinase inhibitors (TKIs) with other kinase inhibitors have shown good response in several cancer types (*6, 29-33*).

We have investigated whether growth of neuroblastoma cell lines harbouring a hyper activated RAS-MAPK pathway is suppressed by the FDA approved MEK inhibitor trametinib, either alone or as a partner in a combinatorial therapy approach. We found that EML4-ALK mutated lung cancer cells and RAS-MAPK pathway mutated neuroblastoma cell lines are sensitive to MEK targeted therapies, however MEK inhibition is not beneficial in ALK addicted neuroblastoma cells with a hyper activated RAS-MAPK pathway. In contrast, in ALK addicted neuroblastoma cells inhibition of MEK results in phosphorylation of the mTORC2 partner SIN1, resulting in an increased survival and growth dependent AKT signalling activity.

Results

Sensitivity of neuroblastoma cell lines to the MEK inhibitor trametinib

Trametinib is a specific and potent MEK inhibitor with IC_{50} of approximately 1-2 nM in cell-free assays (*2-4*). Currently trametinib is involved in several clinical trials (clinicaltrials.gov) either as a single agent or as part of a combinatorial strategy. Trametinib has been suggested to be used with ALK inhibitors, in a rational polytherapy strategy for neuroblastoma. This is a rational approach based upon the robust activation of the RAS-MAPK pathway upon ALK receptor ligation. Thus we set out to test this hypothesis experimentally. Because neuroblastoma is a heterogeneous disease, we first investigated the neuroblastoma cell lines employed in this study defining their characteristics and oncogenic drivers. All cell lines used were subjected to SNP analysis using Affymetrix Cytoscan HD arrays and sequenced for mutations in *ALK*, *RAS* and *p53*. Further, NF-1 and IGFR/IR abundance was investigated (figs. S1 and S2; Table 1, table S1).

We first focused on the CLB-BAR, CLB-GE, CLB-GAR and Kelly neuroblastoma cell lines, that have previously been shown to be ALK addicted (Figure 1) (*23*, *34-36*). The SK-N-AS and SK-N-BE cell lines harbor activating mutations in the *NRAS* gene and exhibit down-regulated NF1 expression, respectively (Table 1 and fig. S1) leading to activation of the RAS-MAPK pathway (*37*). Additional neuroblastoma cell lines employed were IMR32, whose growth can be suppressed by IGF inhibitors (*38*), CLB-PE that harbors a p53 mutation (Table 1) and SK-N-DZ which harbours a p53(R110L) mutation and expresses high levels of activated IGF receptors respectively (fig. S2B; Cosmic database, http://cancer.sanger.ac.uk/cell_lines) (*39*). Because these cell lines have not been sequenced at the whole genome level, additional oncogenic drivers may exist (Table 1).

After genetic characterisation, cell lines were treated with either the MEK inhibitor trametinib (10 nM) or the ALK inhibitor lorlatinib (30 nM). Proliferation was assessed over 12 days. Proliferation of the RAS-activated neuroblastoma cell lines (SK-N-AS and SK-N-BE) was sensitive to trametinib treatment (Figure 1, A and B). In contrast, ALK-positive neuroblastoma cell lines (CLB-BAR, CLB-GE, CLB-GAR and Kelly) continued to grow upon trametinib treatment for at least 12 days (Figure 1, A and B). Increasing the dose to 100 nM, 10-times its IC_{50} value, resulted in growth inhibition of all cell lines tested. In agreement with earlier findings, all ALK-addicted neuroblastoma cells tested exhibited sensitivity to the ALK inhibitor lorlatinib (Figure 1, A and B) (*36*, *40*). We also observed that neuroblastoma cell lines

with mutations in *p53*, such as CLB-PE and SK-N-DZ or high expression of insulin-like growth factor, similar to the IMR32 line, were insensitive to trametinib (Figure 1B).

To further investigate the role of RAS-MEK-ERK signaling, the CLB-BAR and CLB-GE ALK-addicted neuroblastoma cell lines were treated with low nanomolar amounts of either with trametinib alone, lorlatinib alone or a combination of both (Figure 1, C and D). The combination of different concentrations of trametinib and lorlatinib did not result in synergistic growth inhibition in ALK-positive neuroblastoma cell lines when compared to mono-treatment (Figure 1, C and D, and Table S2).

Thus, these results suggest that neuroblastoma cell lines exhibiting ALK-addicted, high-*IGFR* expressing, and *TP53*-deleted characteristics are not primarily dependent on RAS-MAPK pathway signalling for survival/proliferation. In contrast, neuroblastoma cell lines harbouring direct RAS-MAPK pathway aberrations, such as RAS mutation or NF1 loss, are sensitive to trametinib.

AKT pathway dependence in ALK-positive neuroblastoma cell lines

We next set out to investigate the mechanisms underlying the lack of sensitivity of ALK addicted neuroblastoma cell lines to MEK inhibition. Given that earlier observations have indicated that the PI3K/mTOR/ERK5 signaling complex is important for the survival of ALK-addicted neuroblastoma cells (*32, 33*), we investigated activity of the AKT-mTOR-ERK5 pathway in response to trametinib treatment. Upon treatment with trametinib, ALK-addicted cell lines exhibited a 2-fold increased phosphorylation/activation of both AKT and ERK5 (Figure 2, A, B and C). A similar increase in AKT activity was observed in the Kelly cell line (fig. S3A) and the p53 mutated cell lines SK-N-DZ and CLB-PE (fig. S3C) but not in the RAS-MAPK pathway-mutant cell lines, SK-N-AS and SK-N-BE (fig. S3D). To further evaluate the dependence of AKT-ERK5 signalling, we treated CLB-GE and CLB-BAR with PI3-K (BEZ235) and ERK5 (XMD8-92) inhibitors. Both PI3K and ERK5 inhibitors reduce the phosphorylation levels of AKT(S473) and ERK5(T218/Y220), respectively, however, no difference of the phosphorylation status of MAPK was observed (fig. S4A). Together, our data reveal the importance of AKT signalling core in ALK-positive neuroblastoma cells that is potentiated in response to MEK inhibition.

Increased activation of AKT from ligand mediated activation of ALK upon treatment with trametinib.

ALKAL1 (FAM150A, AUGβ) and ALKAL2 (FAM150B, AUGα) are potent ligands for ALK (*41-43*), prompting us to investigate the effect of trametinib inhibition on ALK signalling in response to ALKAL1 stimulation. We used the IMR-32 neuroblastoma cell line, which harbours a ligand responsive ALK in which exon 2-4 of ALK are amplified (Table 1). In agreement with our previous findings (*41*), we observed that stimulation of IMR-32 cells with ALKAL1 led to the phosphorylation of both AKT (Ser^{473}) and ERK5 (Thr^{218}/Tyr^{220}) that was abrogated in the presence of the ALK inhibitor lorlatinib in combination with trametinib (Figure 2D). Similar results were observed employing the ALK-addicted cell line, CLB-GE (fig. S4B). In contrast, in ALKAL1-stimulated IMR32 cells inhibition of MEK with trametinib increased the phosphorylation of both AKT and ERK5 close to two-fold and reduced the phosphorylation of ERK1/2. This increase in AKT and ERK5 phosphorylation was dependent on ALK activity, because lorlatinib inhibited this response and treatment of IMR32 cells with trametinib alone showed no increase in either AKT or ERK5 phosphorylation (Figure 2D). These results indicate that the activity of the ALK itself is important in the increased activation of AKT signalling core in response to trametinib.

We next asked whether this response was unique to ALK-addicted neuroblastoma cells, investigating the effect of trametinib on AKT signalling in the EML4-ALK–positive H3122 and DFCI032 NSCLC cell lines. Proliferation and AKT signaling were examined in both H3122 and DFCI032 cells after treatment with either trametinib or lorlatinib. In contrast to ALK-addicted neuroblastoma cells, we observed that (i) both EML4-ALK–positive H3122 and DFCI032 NSCLC cells were sensitive to trametinib, and (ii) the increased activation of AKT signaling seen upon trametinib treatment in ALK-addicted neuroblastoma cells was not observed in EML4-ALK-positive H3122 or DFCI032 cell lines (fig. S5, A and B). These data suggest that, in contrast to the efficacy of trametinib in ALK-positive NSCLC, the increased activation of the AKT signaling core observed in ALK-positive neuroblastoma cells potentiates ALK signaling output.

mTORC2 drives increased activation of AKT in ALK-positive neuroblastoma cells.

Reactivation of RTK signaling is a plausible mechanism of increased AKT activation after MEK inhibition. However, we performed a phospho-RTK array on lysates from ALK-addicted neuroblastoma cell lines after treatment with trametinib and found no significant reactivation of any RTK (fig. S6A). Another possible mechanism for reactivation of or enhanced signaling to AKT is through the RAS-PI3K-AKT pathway; however, no increase in the abundance of RAS-GTP was detected upon treatment of trametinib, although ERK1/2 phosphorylation was decreased (fig. S6B). Upon RAS-mediated PI3K activation, PI3K phosphorylates phosphatidylinositol (4,5)-bisphosphate (PIP2), making phosphatidylinositol (3,4,5)-trisphosphate (PIP3) (*44-46*). PIP3 recruits proteins such as AKT to the membrane through pleckstrin-homology (PH) domain-mediated binding, leading to activation upon binding to newly formed PIP3. However, similar to the RAS-GTP assay, no increase or decrease in the PIP3/PIP2 lipid ratio was observed upon treatment with trametinib, whereas treatment with lorlatinib (the ALK inhibitor) lowered the PIP3/PIP2 ratio (fig. S6C). These observations suggest that crosstalk between the MAPK and AKT signaling pathways may be responsible for the increased activation of the AKT signalling core in response to MEK inhibition.

We next determined whether activation of AKT signaling in ALK-addicted neuroblastoma cells in response to trametinib involves the mTOR complexes that have previously been described as master feedback regulators (*47, 48*) by combining trametinib treatment in ALK-addicted neuroblastoma cell lines (CLB-BAR, CLB-GE, CLB-GAR and Kelly) with the PI3K inhibitor BEZ235, the mTORC1 and mTORC2 inhibitor AZD8055, or the mTORC1 inhibitor everolimus. As single applications, PI3K and mTORC1/2 inhibition (using BEZ235 and AZD8055, respectively) efficiently blocked the activation of AKT (inferred by phosphorylation at Ser^{473}), but blocking mTORC1 using everolimus increased AKT activation similar to that seen with trametinib (Figure 3A, **and fig. S3, A and B**). Trametinib alone blocked the phosphorylation (activation) of ERK but not of p70S6K, whereas BEZ235, AZD8055 and everolimus blocked p70S6K but not the activation of ERK (Figure 3A, **and fig. S3, A and B**). Treatment with everolimus increased the activation of AKT, indicating a certain role for mTORC1 in this feedback loop (Figure 3A, **and fig. S3, A and B**). Together trametinib and everolimus appeared to have an additive effect on the activation status of AKT (Figure 3A, **and fig. S3, A and B**). Further, increased activation of AKT (phosphorylation at Ser^{473}) after MEK inhibition was independent of the phosphorylation of

mTORC2 complex protein Rictor (at Thr^{1135}) (Figure 3A, **and fig. S3, A and B**). Furthermore, PI3K or mTORC1/2 inhibitors abrogated trametinib-induced activation of AKT, whereas the mTORC1-selective inhibitor everolimus did not (Figure 3A, **and fig. S3, A and B**), suggesting a role for mTORC2 in the increased activation of AKT signaling in ALK-addicted neuroblastoma cell lines. Assays with the structurally dissimilar mTOR kinase inhibitors rapamycin (an mTORC1 inhibitor) and KU-0063794 (an mTORC1/2 inhibitor) further supported a role for mTORC2 (fig. S7).

To confirm the involvement of mTORC2 complex in the increased activation of AKT signaling core in ALK-addicted neuroblastoma cell lines upon treatment with trametinib, we inhibited mTORC2 activation using small interference RNA (siRNA) targeting the mRNA encoding Rictor (Figure 3B). Compared with cells transfected with control siRNA, cells transfected with one of two independent Rictor siRNAs decreased the basal activation of AKT (Figure 3B). In response to trametinib, AKT activation increased in control but not Rictor siRNA-transfected ALK-positive neuroblastoma cells (Figure 3B). Together, these results suggest a critical role for mTORC2 proteins in MEK inhibitor-induced activation of AKT signaling.

Blocking MEK-ERK signaling enhances AKT activation through SIN1 phosphorylation.

Our data thus far suggests that RAS-MEK-ERK pathway inhibition in ALK-addicted neuroblastoma cells lead to increased activation of AKT signaling via mTORC2 in a manner that is dependent on the presence of Rictor but independent of its phosphorylation at Thr^{1135}. However, residue Thr^{1135} is important for mTORC2 signaling (*49*), thus we explored additional components of the mTORC2 complex. The mTORC2 complex includes Rictor, Stress-activated protein kinase (SAPK) interacting protein 1(SIN1) and lethal with SEC13 protein 8 (LST8). We started with SIN1, a key regulator of mTORC2 (*50, 51*). Immunoblotting for phosphorylated SIN1 (at Thr^{86}) in ALK-addicted neuroblastoma cell lines CLB-BAR and CLB-GE revealed that MEK or ERK1/2 inhibition (with trametinib or SCH772984, respectively) increased phosphorylation of SIN1 , but that PI3K inhibition (with BEZ235) alone or in combination with either the MEK or ERK1/2 inhibitor reduced SIN1 phosphorylation (Figure 4A). These observations together with the results from treatment with AZD8055 inhibitor (Figure 3A) suggest that RAS-MEK-ERK inhibitor-induced activation of AKT in ALK-addicted neuroblastoma cells occurs through phosphorylation of SIN1 . Further

supporting the involvement of SIN1, knockdown of SIN1 expression using RNA interference inhibited trametinib (MEK inhibitor)-induced AKT activation in ALK-addicted neuroblastoma cells (Figure 4B).

Together, our results indicate that RAS-MEK-ERK pathway inhibition leads to an increased activation of AKT signaling via increased SIN1 Thr^{86} phosphorylation in ALK-addicted neuroblastoma cells.

Treatment with trametinib abrogates tumor growth in ALK-positive NSCLC xenografts but not ALK-addicted neuroblastoma xenografts.

The effect of trametinib was evaluated in BalbC/NUDE mice subcutaneously injected with either human neuroblastoma cells (CLB-BAR or SK-N-AS), or EML4-ALK NSCLC cells (H3122). Treatment of mice (by oral gavage) with trametinib inhibited the growth of NSCLC xenografts as well as that of RAS-mutant SK-N-AS neuroblastoma xenografts (Fig. 5, A and B), similar to the observed inhibition of proliferation in our in vitro assays above and as in earlier reported xenografts (*9, 11*). In contrast, tumor growth inhibition of ALK-addicted CLB-BAR neuroblastoma xenografts was not observed on trametinib treatment when compared to vehicle-treated mice (Figure 5C). Further, immunoblotting revealed increased AKT phosphorylation in CLB-BAR xenografts excised from mice treated with trametinib, although a decreased phosphorylation of ERK1/2 was observed (fig. S8A), in line with our findings in the cultured cells (Figures. 2 and 3). No sign of distress in the mice was observed upon treatment with trametinib, and the mean bodyweights in the vehicle and drug-treated mice were not significantly different (fig. S8B**).** Thus, while treatment with trametinib is beneficial in tumors harboring ALK fusion protein-driven NSCLC and RAS-mutant neuroblastoma xenografts, it exhibits no beneficial effect on ALK-addicted neuroblastoma xenografts.

Discussion

Whereas monotherapy for cancers with ALK-fusions shows promising results, the response of ALK-positive neuroblastoma patients to ALK TKIs as a monotherapy is less encouraging, as reported for crizotinib (*5, 52*). Lately, new suggestions have appeared from the neuroblastoma field with support from studies using EML4-ALK NSCLC cells that

combined inhibition of ALK and the MEK-ERK pathway may be beneficial as poly-therapy in neuroblastoma patients (*8, 9, 11, 53, 54*). However, our results with various neuroblastoma cell lines suggest that use of MEK inhibitors is not effective as a single or a poly-therapeutic strategy in ALK-positive neuroblastoma. .

RTKs signal to both the PI3K and the MAPK pathway, and crosstalk between these two pathways are common, in which inhibition of either pathway can lead to activation of other pathways (*55-57*). One possible mechanism upon inhibition of MAPK proteins could be an increased activity of PI3K via Ras-GTP, however in our hands no increased PI3K activity was observed(*44-46*). Further, a number of feedback mechanisms have been proposed, such as the RAF paradox in melanoma (*6, 58-62*) and involvement of RTKs in the feedback activation mechanisms (*62, 63*). Other studies have indicated the importance of mTOR kinases and their enigmatic complex activation (*30, 61, 64-67*). There are two different mTOR complexes, mTOR complex 1 (mTORC1) and 2 (mTORC2), that respond to different cues, such as growth factors and nutrient availability. Dysregulation of mTOR complexes has been observed in many diseases, such as cancer, obesity and diabetes (*66*). The mTORC2 complex consists of mTOR subunit, Rictor, SIN1, mLST8 and Protor and its complex regulation is unresolved. Recently it was shown that the mTORC2 subunit SIN1 is an AKT substrate in 3T3-L1 adipocytes and HEK293 cells, which positively regulates mTORC2 activity (*68*). It has also been reported that in HeLa cells S6K is responsible for phosphorylation of SIN1 in a negative feedback loop between mTORC1 and C2 that inhibits mTORC2 activity (*51*). Studies have indicated that phosphorylation of SIN1 at T86 increases the kinase activity of mTORC2, leading to phosphorylation of AKT on S473 site (*67*). We observed that inhibition of the RAS-MAPK pathway resulted in an increased activation of AKT in ALK-addicted neuroblastoma cell lines, likely occurring through the mTORC2 complex, and identify SIN1 Thr^{86} phosphorylation of mTORC2 as an important molecular event. Further, reduction of SIN1 expression decreases phosphorylation of AKT on residue 473.

Previous studies have reported that increased AKT phosphorylation after mTORC1 inhibition is dependent upon phosphorylation of Rictor at Thr^{1135} (*65, 69*), which is in agreement with our results here. We also found that Rictor was required as a partner in the mTORC2 but that phosphorylation of Rictor at Thr^{1135} was not necessary for the increased phosphorylation of AKT after MEK inhibition. A similar increase in AKT phosphorylation was reportedly observed after MEK inhibition in *HER2*-amplified and *EGFR*-mutant cancer cells as a result of ERBB receptor signaling (*62*). Another report found that long-term treatment of

breast cancer cells with inhibitors that block both mTORC1 and mTORC2 induced the activation of PI3K–AKT signaling and increased protein levels of EFGR, HER2 and HER3 and IRS1(*63*). A challenging but critical task toward optimizing therapeutic strategies is to understand these complex molecular mechanisms in an individual tumor.

Our results in neruoblastoma cells are in contrast to the behaviour of EML4-ALK fusion protein-addicted NSCLC lines that are sensitive to MEK and ERK1/2 inhibitors and do not mediate an increased activation of the AKT protein, consistent with previous reports (*9*). The reason behind this phenomenon is unclear; however, the oncogenic activity of the fusion proteins, such as EML4-ALK, is still dependent on oligomerization and activation driven by the EML4 fusion partner. In contrast, the full length ALK receptor is located in membranes, it can be further activated by ligands, such as in the IMR32 cell line, although tested cell lines here harbor a receptor with ligand-independent ALK activity. Further, abrogating PI3K or ERK5 signaling does not increase activation of MAPK pathway in ALK-addicted cell lines (fig. S4A). Abrogation of both ALK and PI3K or ERK5 activity synergistically reduce neuroblastoma cell proliferation and tumor growth (*32, 33*). It has been suggested that increased AKT signalling could attenuate anticancer efficacy, confer resistance, and/or contribute to the development of resistance (*47, 48*). Further, reducing mTORC2 activity decreases HIF2α mRNA and protein expression correlating with smaller and less vascularized tumours from metastatic tumor xenografts (*70*).

Future investigation will be needed to clarify whether MEK or ERK1/2 are responsible directly or indirectly for the phosphorylation of Thr^{86} of SIN1 at the molecular level. Alternatively, they may negatively regulate a SIN1 phosphatase mediating the cross-talk mechanisms between RAS-MAPK pathway and mTORC2. An additional hypothesis is that MEK-ERK mediate a negative feedback loop on SIN1, since the phosphorylation status of RICTOR, a mTORC2 complex member, at residue 1135 does not appear to be important in ALK-positive neuroblastoma and has been reported not to affect mTORC2 kinase activity (*49, 69, 71, 72*).

In this work we show that treatment of ALK-addicted neuroblastoma cells or xenografts with MEK/ERK inhibitor does not abrogate cell or tumour growth. Our data is supported by a reports indicating that other ALK-addicted cell lines do not respond to binimetinib, an orally bioavailable inhibitor of MEK1/2 (IC_{50} = 12 nM) as a single agent or in combination with ALK inhibitor, although binimeinib is an effective inhibitor against neuroblastoma tumour cells with

activated RAS or low NF1 expression (*12, 13, 73*). Our results highlight a mechanism upon MEK/ERK inhibition in an ALK addicted neuroblastoma background, as treatment results in an increased activation of AKT–ERK5 signaling under these circumstances. These results indicate that combination of ALK inhibitors with MEK/ERK inhibitors are not motivated as treatment option for ALK-addicted neuroblastoma in the clinic, reflecting the need to fully understand the complex molecular mechanisms involved before considering combinatorial treatment in neuroblastoma patients.

Materials and Methods

High-resolution single nucleotide polymorphism (SNP) array

DNA from nine cell lines was analyzed for copy number changes using CytoScan® HD (Affymetrix Inc., Santa Clara, CA). CytoScan® HD with approximately 2,7 milj probes, has a mean marker distance of 1marker/1kbp. The cell lines were CLB-BAR, CLB-GE, CLB-GAR, Kelly, SK-N-DZ, CLB-PE, IMR32, SK-N-AS and SK-N-BE. All CLB-lines are from Centre Leon Berard, France under MTA. The array experiments were performed according to the protocol provided by the supplier. Briefly, total genomic DNA (250 ng) was digested with the restriction enzyme and ligated to adaptors. After ligation, the template was subjected to PCR amplification using a generic primer that recognizes the adaptor sequence. The purified PCR products was fragmented with DNase I, labeled with biotin and hybridized to a GeneChip Human Mapping array. The hybridized probes were washed using the Affymetrix Fluidics Station 450 and marked with streptavidin-phycoerythrin. The arrays were scanned using a confocal laser scanner, GeneChip Scanner 3000 (Affymetrix. GeneChip® operating software (GCOS) and GeneChip® Genotyping Analysis Software (GTYPE; Affymetrix) were used for primary data analysis, normalization against internal control features on the chip, genotype calling and quality control. Subsequent analysis was then performed using Copy Number Analyzer for GeneChip (CNAG 3.5.1; Genome Laboratory, Tokyo University) [http://www.genome.umin.jp] featuring the algorithm for Allele-specific Copy-Number analysis using Anonymous References (AsCNAR). In CNAG, the tumor samples were compared in silico to the 8 best matched control samples (lowest standard deviation) available among a set of non-matched healthy individuals. This set contained both HapMap samples available from Affymetrix as well as our own set of healthy control samples. We also used Chromosome Analysis Suite software (ChAS v. 2.0.0.195; Affymetrix) for performing the cytogenetics analysis. All cases of chromosomal gain, loss, or amplification were scored for both segmental and numerical aberrations, including detailed information about the breakpoint positions when applicable. Chromosomal positions (in Table 2) are given according to human genome build GRCh37/hg19. Determination of genomic profile (Table 1) was done essentially in the same way we have done previously (*74*).

DNA sequencing of *ALK, TP53* and *NRAS* regions according to Sanger

Sanger sequencing was performed for DNAs from the nine cell lines. The sequenced regions were: for ALK exons 21-26 (cover aa positions 1120-1313); for TP53 exons 5-10 (aa

pos. 33-367), and for NRAS exons 2 and 3 (cover aa positions 1-97). Touch-down PCR was performed in 10µl reactions using AmpliTaq Gold DNA Polymerase (ThermoFisher scientific), 10 µM forward and reverse primer respectively and 20 ng of cell line DNA. The PCR programme was performed as follows: 95˚C for 5 min, before 20 cycles of 95˚C for 30 s, 65˚C for 30 s (decreasing by 0.5˚C in every cycle) and 72˚C for 1 min, followed by 16 cycles of 95˚C for 30 s, 55◦C for 30 s and 72◦C for 1 min, and ending with an extension step at 72˚C for 7 min. The specificity of products was inspected by agarose gel electrophoresis before they were purified using Agencourt AMPure magnetic beads (Beckman Coulter) using the Biomek NX pipetting robot (Beckman Coulter) and eluted in distilled H_2O. Sequence PCR was performed using the BDT (BigDye Terminator) v3.1 Cycle Sequence Kit (Applied Biosystems) in 10µl reactions containing 6µl of 1:3 diluted PCR/template DNA and 1µl each of BDT, 1×BDT buffer and 1.6µM forward and reverse PCR primer. Sequence PCR was run under the following conditions: 94˚C for 3 min, followed by 50 cycles of 96˚C for 30 s, 50˚C for 10 s and 60˚C for 3 min each. Sequencing products were purified using CleanSeq magnetic beads (Agencourt) using the Biomek NX and re-suspended in High Dye formamide (10 µl; Applied Biosystems). Sequencing products were separated with gel electrophoresis on a 3730 DNA analyser (Applied Biosystems) and the output data were viewed and analyzed using SeqScape v2.5 (Applied Biosystems). All of the fragments were analyzed with both forward and reverse primers and all of the findings were confirmed by sequencing of a new PCR product. Sequencing was performed in house or at GATC biotech AG, European custom Sequencing Center (Germany).

Antibodies, Cell lines and Reagents

Pan-ERK1/2 antibody (1:5000; Cat# 610123), was purchased from BD Transduction Laboratories (Franklin Lakes, NJ), phospho-ALK (1:1000; Y1604; #3341), phospo-ERK5 (1:1000; T218/Y220; Cat# 3371), ERK5 (1:2000; Cat# 3372), phospho-AKT (1:5000; Ser473; #4060), AKT (1:10000; Cat# 9272), Rictor (1:1000; #2114), phospho-Rictor (1:1000; T1135; #3806), SIN1 (1:000; #12860), phospho-SIN1 (1:1000; T86; #14716), phospho-p70 S6 kinase (1:1000; Thr389; #9234), S6K (1:2000; Cat# 9202), p44/42 MAPK (1:5000; ERK1/2; #9102), β-Actin (1:10000; #4970), and tubulin (1:10000; #2144) antibodies were from Cell Signaling Technology. Horseradish peroxidase (HRP)-conjugated secondary antibody, goat anti-mouse IgG, and goat anti-rabbit IgG (1:5000) were purchased from Thermo Scientific. ALKAL

(FAM150A) was used as described previously (*41*). Trametinib, SCH772984**,** BEZ235**,** AZD8055**,** XMD8-92**,** Everolimus (RAD001) were from Selleckchem. The H3122 and DFCI032 cell lines were a kind gift from R. George and P. Jänne, Dana-Farber Cancer Institute. All neuroblastoma and NSCLC cell lines were cultured in RPMI 1640 or DMEM with 10% FBS and 1% penicillin and streptomycin.

Immunoblotting

Cells were lysed on ice with hypotonic lysis buffer (20 mM Tris-HCl (pH 7.5), 150 mM NaCl, 1 mM EDTA, 1 mM EGTA, 1% Triton, 2.5 mM sodium pyrophosphate, 1 mM beta-glycerophosphate, 1 mM Na_3VO_4, 1 µg/ml leupeptin with protease/phosphatase inhibitor cocktail (Cell Signaling Technology)) for 15 minutes and then centrifuged for 10 minutes at 4°C. The proteins was separated on 7.5% Bis-Acryl-Tris gels, transferred to PVDF membranes (Millipore), blocked in 5% BSA (phosphoprotein blots) or 5% milk, and immunoblotted against primary antibodies overnight at 4°C. Secondary antibodies were diluted 1:10,000 and incubated, shaking, at room temperature for 1 hour. Enhanced chemiluminescence substrates were employed for detection (GE Healthcare). Antibody dilutions are noted in the section above.

Viability assay

Cell viability was assessed as relative redox metabolic activity using a resazurin-based assay. CLB-BAR, CLB-GE, CLB-GA, Kelly, SK-N-AS, SK-N-BE, SK-N-DZ, IMR32 and CLB-PE neuroblastoma cells (0.2×10^5) were plated on collagen-coated 24-well plates. Cells were treated with inhibitors as indicated in the figures and monitored for 12 days, refreshing the media and inhibitor dose every third day. Cells were incubated with 55 µmol/l Resazurin (Sigma, Stockholm, Sweden) for 3 hours at 37˚C. Metabolized Resazurin was analyzed by plate reader (TEKAN, Männedorf, Switzerland) as relative fluorescence. For combination treatments 0.4×10^5 cells were plated on collagen-coated 48-well plates, treated as indicated in the figures, and monitored for 5 days. Cell viability was assessed as described for single-inhibitor assays.

SiRNA Transfection

CLB-BAR and CLB-GE cell lines were transfected with one of two duplex siRNAs targeting *RICTOR* and *SIN1* (Stealth RNAi: Invitrogen) according to the manufacturer's protocols. Cells transfected with scrambled siRNA (Invitrogen) were used as negative controls.

Phospho-RTK array

ALK-positive neuroblastoma cell line lysates (400 µg) were incubated on human phospho-Receptor Tyrosine Kinase membrane array according to manufacturer's instruction (ARY001B, R&D systems). Phospho-RTK abundances were assessed using HRP-conjugated pan-phosphotyrosine antibody followed by chemiluminescence detection.

PIP mass quantification

Phospholipids were isolated from CLB-BAR neuroblastoma cells and PIP abundance was measured using an enzyme-linked immunosorbent assay (ELISA) kit (Echelon Biosciences) according to the manufacturer's protocol.

Active Ras assay

For detecting active Ras, cells were plated on 10cm plate and treated with trametinib for 3 hours. Active Ras was measured using active Ras detection kit (Cell Signalling) according to manufacturer's protocol.

Subcutaneous xenografts.

BALB/cAnNRj-Foxn1nu, females (Janvier lab, France) at 5-6 weeks age were subcutaneously injected with cells, 2.5 x 10^6 CLB-BAR, H3122 or SK-N-AS cells in serum free media mixed 1:1 with Matrigel® Matrix (Corning, Lot#6140322), total injection volume 100 µl, into the left flank. Once tumor volume reached an average of 100-150mm^3, the mice were randomized to treatment groups. Drug was given at 3 mg/kg body weight, by oral gavage, daily, continuously for 12 days. Tumor volume was measured by calipers every other day and calculated by the following equation: $V= (\pi/6)\times L\times W^2$ (V=volume, L=longest, W=width). The vehicle for trametenib was 10% Kollisolv® PEG E 400 (Sigma, 06855, Lot.#BCBQ6662V) and 10% Kolliphor® EL(Sigma, C5135, Lot. #BCBQ5632V).

Statistical analysis

Statistical analyses of the data were performed by Student's paired *t* test. All quantitative analysis were presented as means ± SD as indicated. Measurements were log-transformed to meet normality assumption before analyses. *P* values <0.05 were considered significant.

Supplemental Materials

REFERENCES AND NOTES

1. D. Fey, D. Matallanas, J. Rauch, O. S. Rukhlenko, B. N. Kholodenko, The complexities and versatility of the RAS-to-ERK signalling system in normal and cancer cells. *Semin Cell Dev Biol* **58**, 96-107 (2016).
2. H. Abe *et al.*, Discovery of a Highly Potent and Selective MEK Inhibitor: GSK1120212 (JTP-74057 DMSO Solvate). *ACS Med Chem Lett* **2**, 320-324 (2011).
3. A. G. Gilmartin *et al.*, GSK1120212 (JTP-74057) is an inhibitor of MEK activity and activation with favorable pharmacokinetic properties for sustained in vivo pathway inhibition. *Clin Cancer Res* **17**, 989-1000 (2011).
4. T. Yamaguchi, R. Kakefuda, N. Tajima, Y. Sowa, T. Sakai, Antitumor activities of JTP-74057 (GSK1120212), a novel MEK1/2 inhibitor, on colorectal cancer cell lines in vitro and in vivo. *Int J Oncol* **39**, 23-31 (2011).
5. Y. P. Mosse *et al.*, Safety and activity of crizotinib for paediatric patients with refractory solid tumours or anaplastic large-cell lymphoma: a Children's Oncology Group phase 1 consortium study. *Lancet Oncol* **14**, 472-480 (2013).
6. E. M. Tricker *et al.*, Combined EGFR/MEK Inhibition Prevents the Emergence of Resistance in EGFR-Mutant Lung Cancer. *Cancer discovery* **5**, 960-971 (2015).
7. K. R. Bosse, J. M. Maris, Advances in the translational genomics of neuroblastoma: From improving risk stratification and revealing novel biology to identifying actionable genomic alterations. *Cancer*, (2015).
8. T. F. Eleveld *et al.*, Relapsed neuroblastomas show frequent RAS-MAPK pathway mutations. *Nat Genet* **47**, 864-871 (2015).
9. G. Hrustanovic *et al.*, RAS-MAPK dependence underlies a rational polytherapy strategy in EML4-ALK-positive lung cancer. *Nat Med* **21**, 1038-1047 (2015).
10. M. K. Kiessling *et al.*, Targeting the mTOR Complex by Everolimus in NRAS Mutant Neuroblastoma. *PLoS One* **11**, e0147682 (2016).
11. E. Manchado *et al.*, A combinatorial strategy for treating KRAS-mutant lung cancer. *Nature* **534**, 647-651 (2016).
12. S. E. Woodfield, L. Zhang, K. A. Scorsone, Y. Liu, P. E. Zage, Binimetinib inhibits MEK and is effective against neuroblastoma tumor cells with low NF1 expression. *BMC cancer* **16**, 172 (2016).
13. L. S. Hart *et al.*, Preclinical Therapeutic Synergy of MEK1/2 and CDK4/6 Inhibition in Neuroblastoma. *Clin Cancer Res* **23**, 1785-1796 (2017).
14. J. M. Maris, Recent advances in neuroblastoma. *N Engl J Med* **362**, 2202-2211 (2010).
15. J. M. Maris, M. D. Hogarty, R. Bagatell, S. L. Cohn, Neuroblastoma. *Lancet* **369**, 2106-2120 (2007).
16. K. K. Matthay *et al.*, Neuroblastoma. *Nat Rev Dis Primers* **2**, 16078 (2016).

17. J. R. Park *et al.*, Children's Oncology Group's 2013 blueprint for research: neuroblastoma. *Pediatr Blood Cancer* **60**, 985-993 (2013).
18. S. Goto *et al.*, Histopathology (International Neuroblastoma Pathology Classification) and MYCN status in patients with peripheral neuroblastic tumors: a report from the Children's Cancer Group. *Cancer* **92**, 2699-2708 (2001).
19. S. De Brouwer *et al.*, Meta-analysis of neuroblastomas reveals a skewed ALK mutation spectrum in tumors with MYCN amplification. *Clin Cancer Res* **16**, 4353-4362 (2010).
20. T. J. Pugh *et al.*, The genetic landscape of high-risk neuroblastoma. *Nat Genet* **45**, 279-284 (2013).
21. H. Caren, F. Abel, P. Kogner, T. Martinsson, High incidence of DNA mutations and gene amplifications of the ALK gene in advanced sporadic neuroblastoma tumours. *Biochem J* **416**, 153-159 (2008).
22. Y. Chen *et al.*, Oncogenic mutations of ALK kinase in neuroblastoma. *Nature* **455**, 971-974 (2008).
23. R. E. George *et al.*, Activating mutations in ALK provide a therapeutic target in neuroblastoma. *Nature* **455**, 975-978 (2008).
24. I. Janoueix-Lerosey *et al.*, Somatic and germline activating mutations of the ALK kinase receptor in neuroblastoma. *Nature* **455**, 967-970 (2008).
25. Y. P. Mosse *et al.*, Identification of ALK as a major familial neuroblastoma predisposition gene. *Nature* **455**, 930-935 (2008).
26. A. Bellini *et al.*, Deep Sequencing Reveals Occurrence of Subclonal ALK Mutations in Neuroblastoma at Diagnosis. *Clin Cancer Res* **21**, 4913-4921 (2015).
27. T. Martinsson *et al.*, Appearance of the novel activating F1174S ALK mutation in neuroblastoma correlates with aggressive tumour progression and unresponsiveness to therapy. *Cancer Res* **71**, 98-105 (2011).
28. G. Schleiermacher *et al.*, Emergence of new ALK mutations at relapse of neuroblastoma. *J Clin Oncol* **32**, 2727-2734 (2014).
29. Z. Chen *et al.*, Inhibition of ALK, PI3K/MEK, and HSP90 in murine lung adenocarcinoma induced by EML4-ALK fusion oncogene. *Cancer Res* **70**, 9827-9836 (2010).
30. C. Wang *et al.*, Functional crosstalk between AKT/mTOR and Ras/MAPK pathways in hepatocarcinogenesis: implications for the treatment of human liver cancer. *Cell Cycle* **12**, 1999-2010 (2013).
31. Y. K. Yoon *et al.*, Combination of EGFR and MEK1/2 inhibitor shows synergistic effects by suppressing EGFR/HER3-dependent AKT activation in human gastric cancer cells. *Mol Cancer Ther* **8**, 2526-2536 (2009).
32. N. F. Moore *et al.*, Molecular rationale for the use of PI3K/AKT/mTOR pathway inhibitors in combination with crizotinib in ALK-mutated neuroblastoma. *Oncotarget* **5**, 8737-8749 (2014).
33. G. Umapathy *et al.*, The kinase ALK stimulates the kinase ERK5 to promote the expression of the oncogene MYCN in neuroblastoma. *Science signaling* **7**, ra102 (2014).
34. C. Schonherr *et al.*, Activating ALK mutations found in neuroblastoma are inhibited by Crizotinib and NVP-TAE684. *Biochem J*, (2011).
35. J. T. Siaw *et al.*, Brigatinib, an anaplastic lymphoma kinase inhibitor, abrogates activity and growth in ALK-positive neuroblastoma cells, Drosophila and mice. *Oncotarget*, (2016).
36. J. Guan *et al.*, The ALK inhibitor PF-06463922 is effective as a single agent in neuroblastoma driven by expression of ALK and MYCN. *Disease models & mechanisms* **9**, 941-952 (2016).
37. D. Han, B. A. Spengler, R. A. Ross, Increased wild-type N-ras activation by neurofibromin down-regulation increases human neuroblastoma stem cell malignancy. *Genes Cancer* **2**, 1034-1043 (2011).

38. D. W. Coulter, J. Blatt, A. J. D'Ercole, B. M. Moats-Staats, IGF-I receptor inhibition combined with rapamycin or temsirolimus inhibits neuroblastoma cell growth. *Anticancer Res* **28**, 1509-1516 (2008).
39. C. K. Shiau, D. L. Gu, C. F. Chen, C. H. Lin, Y. S. Jou, IGRhCellID: integrated genomic resources of human cell lines for identification. *Nucleic acids research* **39**, D520-524 (2011).
40. N. R. Infarinato *et al.*, The ALK/ROS1 Inhibitor PF-06463922 Overcomes Primary Resistance to Crizotinib in ALK-Driven Neuroblastoma. *Cancer discovery* **6**, 96-107 (2016).
41. J. Guan *et al.*, FAM150A and FAM150B are activating ligands for Anaplastic Lymphoma Kinase. *Elife* **4**, (2015).
42. A. V. Reshetnyak *et al.*, Augmentor alpha and beta (FAM150) are ligands of the receptor tyrosine kinases ALK and LTK: Hierarchy and specificity of ligand-receptor interactions. *Proc Natl Acad Sci U S A* **112**, 15862-15867 (2015).
43. J. Guan *et al.*, Anaplastic lymphoma kinase L1198F and G1201E mutations identified in anaplastic thyroid cancer patients are not ligand-independent. *Oncotarget*, (2016).
44. T. Kodaki *et al.*, The activation of phosphatidylinositol 3-kinase by Ras. *Curr Biol* **4**, 798-806 (1994).
45. L. E. Rameh, L. C. Cantley, The role of phosphoinositide 3-kinase lipid products in cell function. *J Biol Chem* **274**, 8347-8350 (1999).
46. P. Rodriguez-Viciana *et al.*, Phosphatidylinositol-3-OH kinase as a direct target of Ras. *Nature* **370**, 527-532 (1994).
47. N. Hay, The Akt-mTOR tango and its relevance to cancer. *Cancer Cell* **8**, 179-183 (2005).
48. N. Rosen, Q. B. She, AKT and cancer--is it all mTOR? *Cancer Cell* **10**, 254-256 (2006).
49. L. A. Julien, A. Carriere, J. Moreau, P. P. Roux, mTORC1-activated S6K1 phosphorylates Rictor on threonine 1135 and regulates mTORC2 signaling. *Mol Cell Biol* **30**, 908-921 (2010).
50. E. Jacinto *et al.*, SIN1/MIP1 maintains rictor-mTOR complex integrity and regulates Akt phosphorylation and substrate specificity. *Cell* **127**, 125-137 (2006).
51. P. Liu *et al.*, Sin1 phosphorylation impairs mTORC2 complex integrity and inhibits downstream Akt signalling to suppress tumorigenesis. *Nat Cell Biol* **15**, 1340-1350 (2013).
52. Y. P. Mosse *et al.*, Targeting ALK With Crizotinib in Pediatric Anaplastic Large Cell Lymphoma and Inflammatory Myofibroblastic Tumor: A Children's Oncology Group Study. *J Clin Oncol*, JCO2017734830 (2017).
53. G. Hrustanovic, T. G. Bivona, RAS signaling in ALK fusion lung cancer. *Small GTPases* **7**, 32-33 (2016).
54. I. Lambertz *et al.*, Upregulation of MAPK Negative Feedback Regulators and RET in Mutant ALK Neuroblastoma: Implications for Targeted Treatment. *Clin Cancer Res* **21**, 3327-3339 (2015).
55. J. Downward, Targeting RAS signalling pathways in cancer therapy. *Nat Rev Cancer* **3**, 11-22 (2003).
56. J. A. Engelman, J. Luo, L. C. Cantley, The evolution of phosphatidylinositol 3-kinases as regulators of growth and metabolism. *Nat Rev Genet* **7**, 606-619 (2006).
57. M. C. Mendoza, E. E. Er, J. Blenis, The Ras-ERK and PI3K-mTOR pathways: cross-talk and compensation. *Trends Biochem Sci* **36**, 320-328 (2011).
58. R. B. Corcoran *et al.*, EGFR-mediated re-activation of MAPK signaling contributes to insensitivity of BRAF mutant colorectal cancers to RAF inhibition with vemurafenib. *Cancer discovery* **2**, 227-235 (2012).
59. S. J. Heidorn *et al.*, Kinase-dead BRAF and oncogenic RAS cooperate to drive tumor progression through CRAF. *Cell* **140**, 209-221 (2010).
60. B. Sanchez-Laorden *et al.*, BRAF inhibitors induce metastasis in RAS mutant or inhibitor-resistant melanoma cells by reactivating MEK and ERK signaling. *Science signaling* **7**, ra30 (2014).

61. H. P. Soares *et al.*, Dual PI3K/mTOR Inhibitors Induce Rapid Overactivation of the MEK/ERK Pathway in Human Pancreatic Cancer Cells through Suppression of mTORC2. *Mol Cancer Ther* **14**, 1014-1023 (2015).
62. A. B. Turke *et al.*, MEK inhibition leads to PI3K/AKT activation by relieving a negative feedback on ERBB receptors. *Cancer Res* **72**, 3228-3237 (2012).
63. S. M. Chen *et al.*, HSP90 inhibitor AUY922 abrogates up-regulation of RTKs by mTOR inhibitor AZD8055 and potentiates its antiproliferative activity in human breast cancer. *Int J Cancer* **135**, 2462-2474 (2014).
64. L. Bar-Peled, D. M. Sabatini, Regulation of mTORC1 by amino acids. *Trends Cell Biol* **24**, 400-406 (2014).
65. M. Breuleux *et al.*, Increased AKT S473 phosphorylation after mTORC1 inhibition is rictor dependent and does not predict tumor cell response to PI3K/mTOR inhibition. *Mol Cancer Ther* **8**, 742-753 (2009).
66. M. Laplante, D. M. Sabatini, mTOR signaling in growth control and disease. *Cell* **149**, 274-293 (2012).
67. G. Yang, D. S. Murashige, S. J. Humphrey, D. E. James, A Positive Feedback Loop between Akt and mTORC2 via SIN1 Phosphorylation. *Cell Rep* **12**, 937-943 (2015).
68. S. J. Humphrey, D. E. James, M. Mann, Protein Phosphorylation: A Major Switch Mechanism for Metabolic Regulation. *Trends Endocrinol Metab* **26**, 676-687 (2015).
69. C. C. Dibble, J. M. Asara, B. D. Manning, Characterization of Rictor phosphorylation sites reveals direct regulation of mTOR complex 2 by S6K1. *Mol Cell Biol* **29**, 5657-5670 (2009).
70. S. Mohlin *et al.*, PI3K-mTORC2 but not PI3K-mTORC1 regulates transcription of HIF2A/EPAS1 and vascularization in neuroblastoma. *Cancer Res* **75**, 4617-4628 (2015).
71. D. Boulbes *et al.*, Rictor phosphorylation on the Thr-1135 site does not require mammalian target of rapamycin complex 2. *Molecular cancer research : MCR* **8**, 896-906 (2010).
72. C. Treins, P. H. Warne, M. A. Magnuson, M. Pende, J. Downward, Rictor is a novel target of p70 S6 kinase-1. *Oncogene* **29**, 1003-1016 (2010).
73. A. C. Wood *et al.*, Dual ALK and CDK4/6 Inhibition Demonstrates Synergy against Neuroblastoma. *Clin Cancer Res*, (2016).
74. H. Caren *et al.*, High-risk neuroblastoma tumors with 11q-deletion display a poor prognostic, chromosome instability phenotype with later onset. *Proc Natl Acad Sci U S A* **107**, 4323-4328 (2010).
75. S. Fransson *et al.*, Intragenic anaplastic lymphoma kinase (ALK) rearrangements: Translocations as a novel mechanism of ALK activation in neuroblastoma tumors. *Genes Chromosomes Cancer*, (2014).

Acknowledgements: We thank Staffan Nilsson, Dept. of Mathematical Sciences, Chalmers University of Technology, Sweden for help with the statistical analyses. The H3122 and DFCI032 cell lines were kind gifts from R. George and P. Jänne, Dana-Farber Cancer Institute. **Funding:** This work was supported by the Swedish Cancer Society (15/391 to RHP; 15/775to BH, 15/827 to TM), the Swedish Childhood Cancer Foundation (2015-0096 to RHP; 2015-80, and 2014-150 to BH, 2013-102 to TM), the Swedish Research Council (2015-04466 to RHP; BH 521-2012-2831, 521-2014-3031 to TM), the Göran Gustafsson Foundation (RHP) and a SSF Programme Grant (RB13-0204 to RHP, TM and BH). **Authors contributions:** G.U. carried out all the cell and biochemical analyses. D.E.G. and D.C-M. executed the animal experiments. N.J., A.D. and T.M. investigated and verified all the cell lines employed in the study. R.H.P. and B.H. supervised the project and wrote the manuscript together with G.U. **Competing interests:** The authors declare that they have no competing interests. **Data and materials availability: CLB-BAR, CLB-GE, CLB-GA and CLB-PE cell lines** used in this study are under an MTA agreement with the Center Léon Bérard laboratory; Lyon, France.

TABLE 1: Mutation data for the cell lines. Mutation data for selected critical genes for the nine neuroblastoma cell lines used in this study. [a]Genomic profile as defined in (*74*) [b] (*75*) MNA, MYCN amplified. HomZ.,Homozygote. Mut, mutant. Amp, amplification. Expr.,

Cell line	*Genomic profile*[a]	*ALK status (amp, mut ex23-25)*	*MYCN status*	*TP53 status mut ex5-9*	*NRAS status*	*NF1 expr.*
CLB-BAR	MNA	**Amp. whole ALK** exc. part of i3 (nonamp). Note, **exome sequencing shows del ex4-11**[b]	**MYCN amplified**	No mut in TP53	No mut in NRAS	High
CLB-GE	MNA	**ALK amp.** **ALK mut F1174V**	**MYCN amplified**	No mut in TP53	No mut in NRAS	High
CLB-GAR	11q-del	2p gain with break within ALK intron 1 **Mutation R1275Q**	Not MYCN amplified	No mut in TP53	No mut in NRAS	High
Kelly	MNA + 11q-del	No amplification 2p-gain **Mutation F1174L**	**MYCN amplified**	**HomZ. Mut P177T**	No mut in NRAS	High
SK-N-DZ	MNA	No mutation No amplification	**MYCN amplified**	No mut in TP53	No mut in NRAS	Intermediate
CLB-PE	MNA + 11q-del	2p gain No mutation No amplification	**MYCN amplified**	**HomZ. mut C176F**	No mut in NRAS	High
IMR32	MNA	**Amp. of ALK** ex 3-4 only. No mutation	**MYCN amplified**	No mut in TP53	No mut in NRAS	High
SK-N-AS	11q-del	No mutation No amplification	Not MYCN amplified	No mut in TP53	Mut in NRAS: **Q61K**	Low
SK-N-BE	MNA	2p-gain No mutation No amplification	**MYCN amplified**	**HomZ. mut C145F**	No mut in NRAS	Low

Figure Legends

Figure 1. Sensitivity of neuroblastoma cell lines to MEK inhibition by trametinib. **(A and B)** Viability assessed over 12 days using the Resazurin viability assay in neuroblastoma cell lines [CLB-BAR, CLB-GE, CLB-GA, Kelly (A) and SK-N-AS, SK-N-BE, SK-N-DZ, IMR32, CLB-PE (B)] treated with either trametinib or lorlatinib as indicated. **(C and D)** Resazurin assay-based viability in neuroblastoma cell lines CLB-BAR (C) and CLB-GE (D) treated with trametinib alone or combined trametinib and lorlatinib, as indicated. Data are means ± SE of fold relative fluorescence units (RFU) relative to untreated cells from three independent experiments.

Figure 2. Specificity of AKT signaling core components in ALK-positive neuroblastoma cell lines. (A to C) Western blotting for the indicated proteins in lysates from ALK-positive neuroblastoma cell lines CLB-BAR (A), CLB-GAR (B) and CLB-GE (C) treated with trametinib or lorlatinib for the indicated time (6h, hours). **(D)** Immunblotting of lysates from IMR32 cells pretreated with trametinib, lorlatinib or both for 1h then stimulated with ALKAL1 for 30 min. Tubulin (A-C) or total pan-ERK (D) served as loading controls. Data are means ± SE from ≥three independent experiments. *$p < 0.05$; Student's paired *t*-test.

Figure 3. Trametinib treatment activates AKT signalling via mTORC2. ALK-positive neuroblastoma cell lines CLB-BAR and CLB-GE (**A**) were treated with trametinib, BEZ 235, AZD 8055 or everolimus either alone or in combination as indicated. Cell lysates were immunoblotted for p-Rictor (T1135), Rictor, p-p70S6K, S6K, p-AKT (S473), AKT, p-ERK1/2 and ERK1/2 antibodies. Actin was used as a loading control. **(B)** CLB-BAR and CLB-GE cells were transfected with either scrambled control, or two independent siRNAs targeting Rictor prior to treatment with trametinib. Lysates were separated by SDS-PAGE and analyzed for Rictor, p-Rictor (T1135), p-Akt (S473), AKT, p-ERK1/2 and ERK1/2 expression by immunoblotting with Actin as a loading control. Data are means ± SE from at least three independent experiments. *$p < 0.05$; Student's paired *t*-test.

Figure 4. Knock-down of SIN1 suppresses increased activation of AKT after MEK inhibition. (**A**) Immunoblotting in whole cell lysates from neuroblastoma cell lines CLB-BAR and CLB-GE grown in complete growth medium and treated with trametinib, SCH 772984, BEZ 235, or a combination thereof as indicated. (**B**) Immunoblotting in whole cell lysates from CLB-BAR and CLB-GE cells treated with trametinib for 1h after transfection with

scrambled control (siC) or one of two *SIN1*-targeted siRNAs (si1, si3). Lysates were separated by SDS-PAGE and analyzed for Rictor, Sin1, p-Akt (S473), AKT,p-ERK1/2 and ERK1/2 expression by immunoblotting with actin as a loading control. Data are means ± SE from at least three independent experiments. *$p < 0.05$; Student's paired *t*-test.

Figure 5. Efficacy of trametinib in ALK-positive neuroblastoma and NSCLC xenograft models. (A to C) Growth curves of RAS-positive SK-N-AS neuroblastoma (A; $p \leq 0.05$), EML4-ALK-positive H3122 NSCLC (B; $p \leq 0.05$) or ALK-dependent CLB-BAR neuroblastoma (C; not significantly different by Student's paired t-test) xenografts in vehicle-treated and trametinib-treated mice. Data are means ± SD from n=6 mice in each group.

Figure 1. Umapathy G et al., 2017

A.

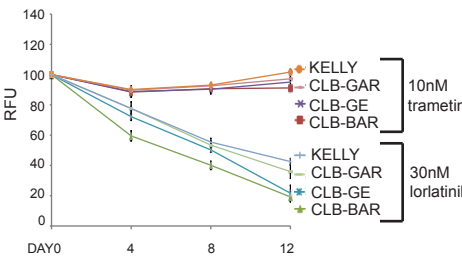

B.

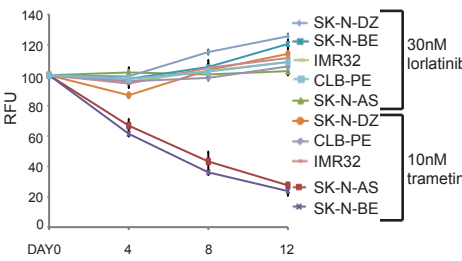

C. CLB-BAR

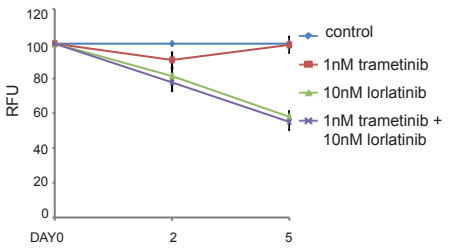

D. CLB-GE

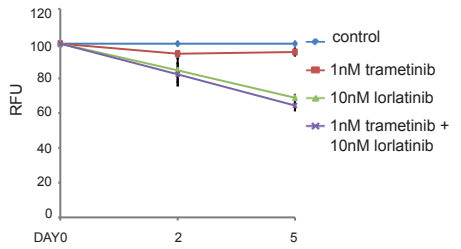

Figure 2. Umapathy G et al., 2017

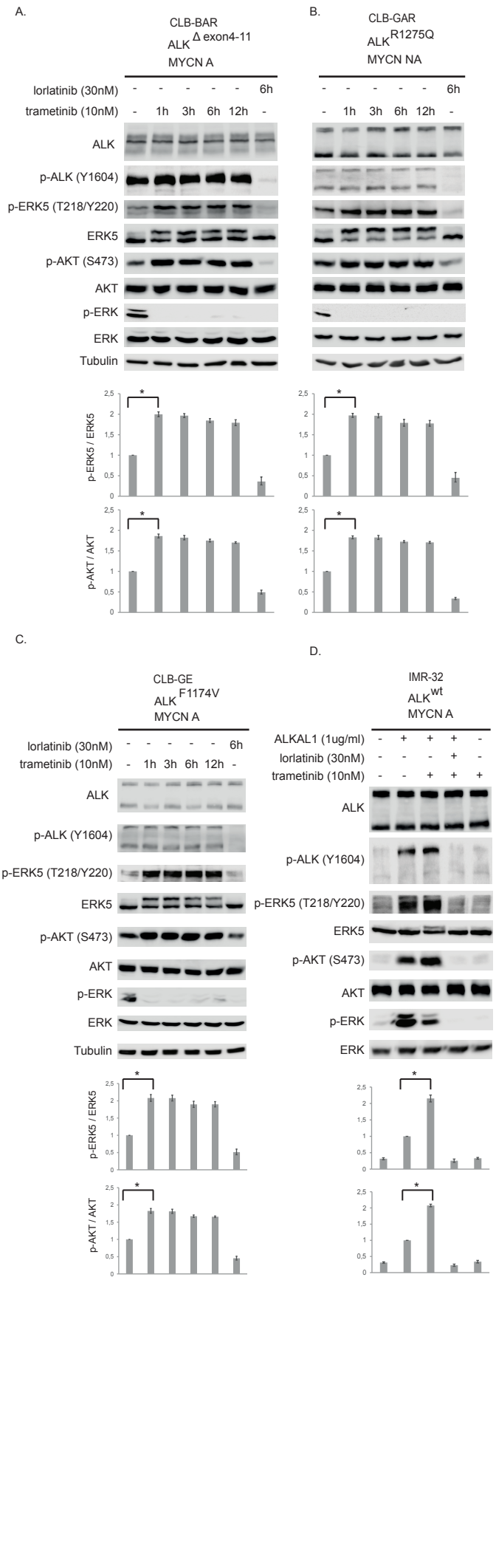

Figure 3. Umapathy G et al ., 2017

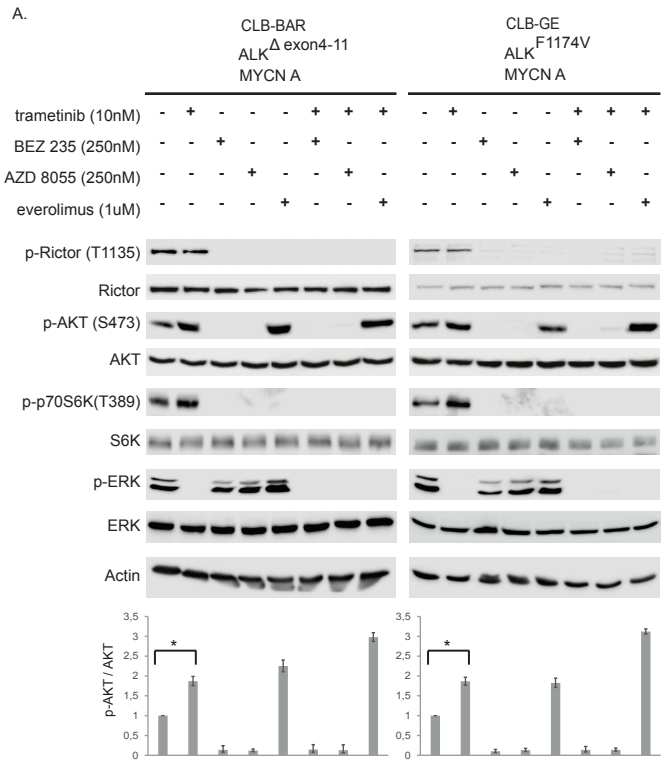

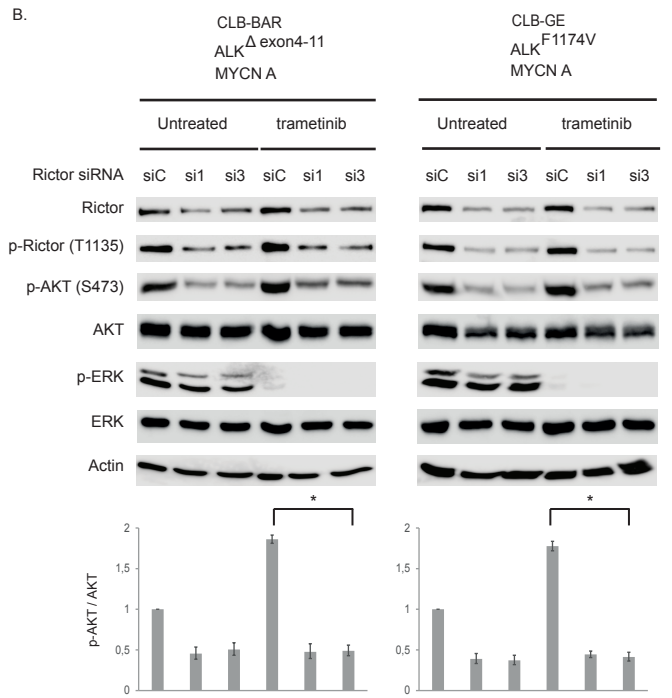

Figure 4. Umapathy G et al ., 2017

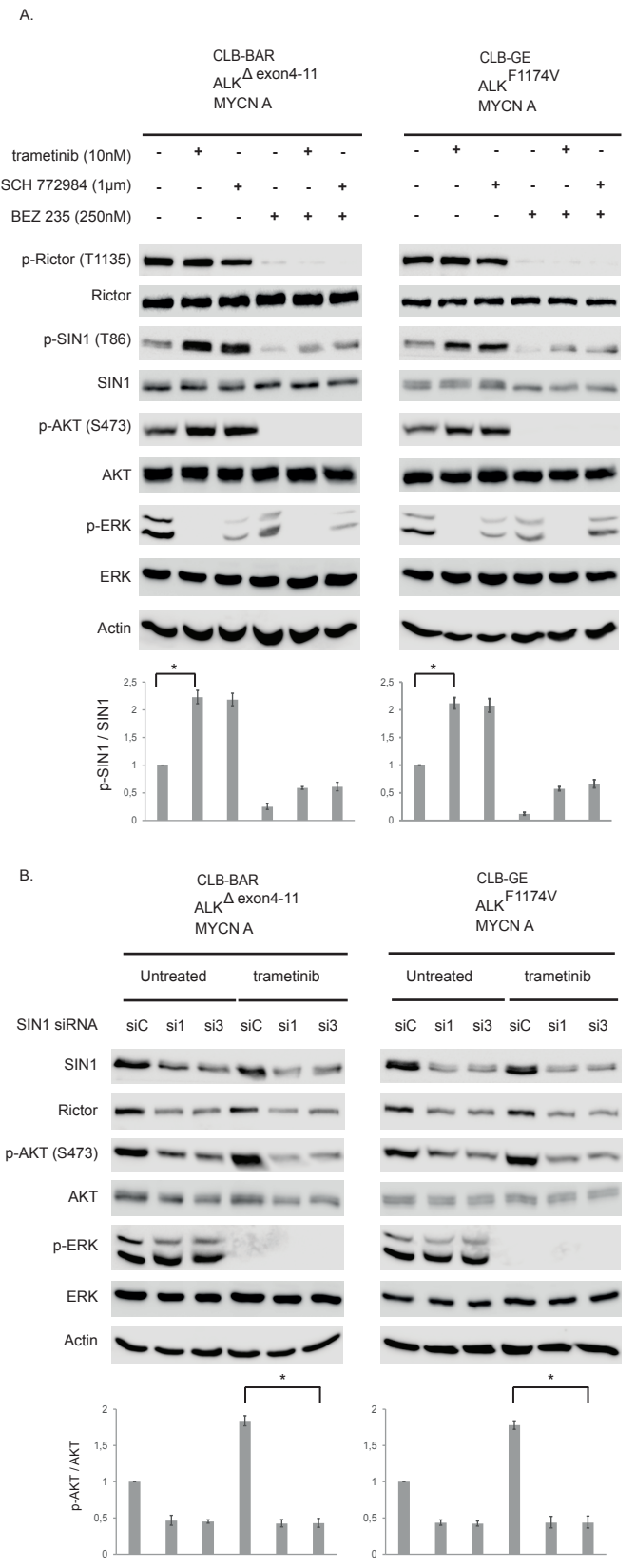

Figure 5. Umapathy G et al., 2017

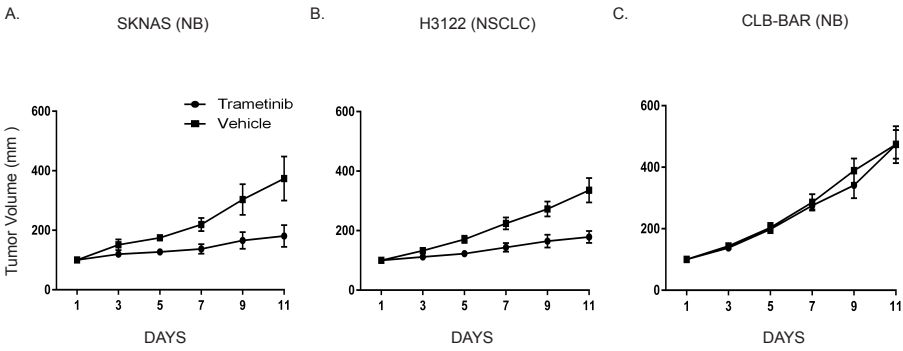

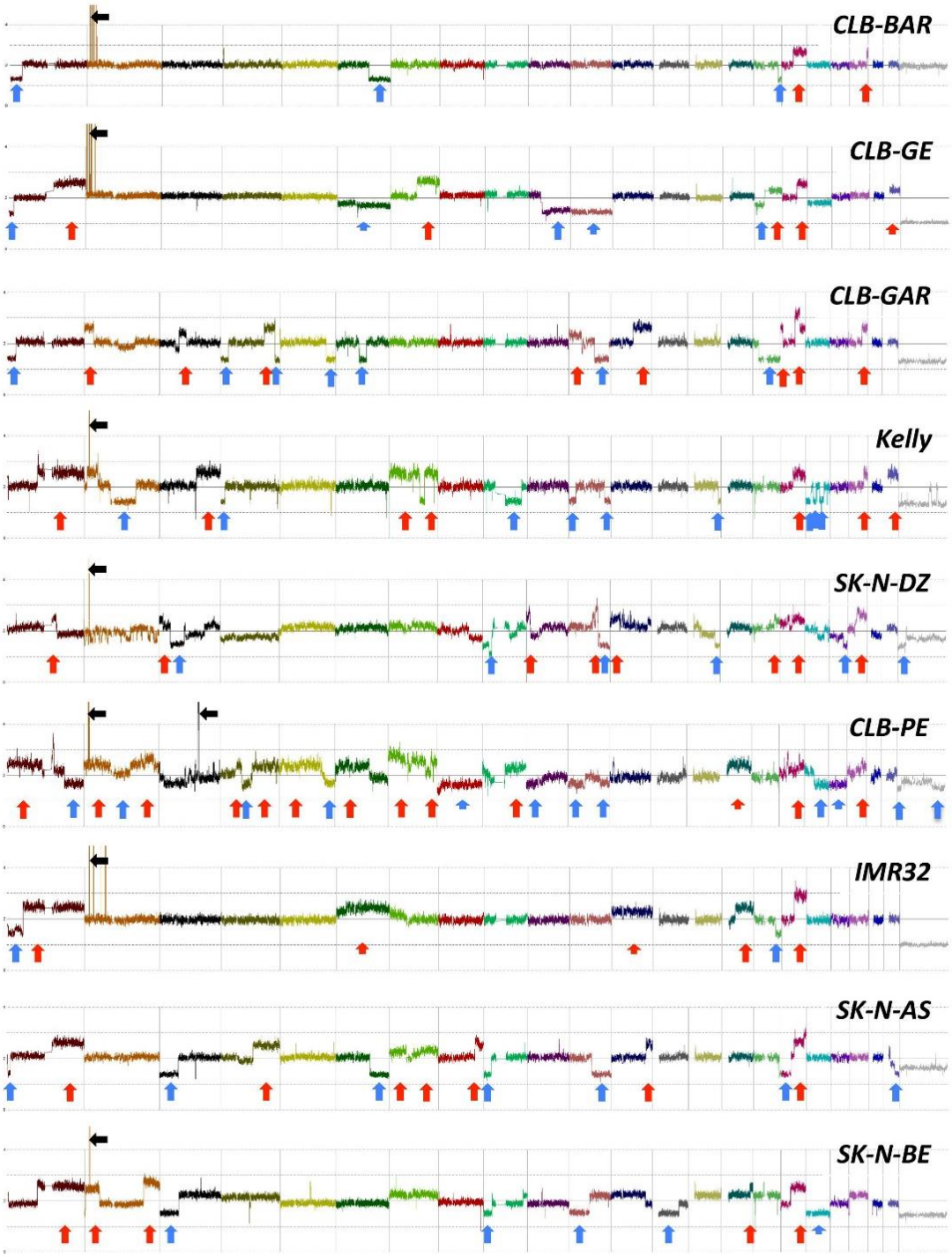

Figure S1. SNP array genome profiles of the nine neuroblastoma cell lines. SNP array genome profiles of the nine neuroblastoma cell lines (labelled right). Arrows indicate copy number changes relative to normal profile: Blue arrows indicate loss of genetic material; red arrows indicate gain of genetic material; black arrows indicate gene amplification. Within that color scheme, shorter arrows indicate numerical changes, whereas longer arrows indicate segmental changes.

Cell Lines	trametinib	lorlatinib	CI value	Effect
CLB-BAR	**0.5nM**	**5nM**	**1.00**	**Antagonism**
CLB-GE	**0.5nM**	**5nM**	**0.96**	**Additive**
CLB-BAR	**1nM**	**10nM**	**1.09**	**Antagonism**
CLB-GE	**1nM**	**10nM**	**1.06**	**Antagonism**
CLB-BAR	**2nM**	**10nM**	**1.11**	**Slight Antagonism**
CLB-GE	**2nM**	**10nM**	**1.10**	**Antagonism**
CLB-BAR	**3nM**	**15nM**	**1.23**	**Moderate Antagonism**
CLB-GE	**3nM**	**15nM**	**1.16**	**Slight Antagonism**

Table S2: Trametinib does not act synergistically with lorlatinib to inhibit ALK-positive neuroblastoma cell line proliferation. After 5 days of treatment, viability curves were generated using Resazurin assay. Drug combination effects were defined using the Combinatory Index (CI) calculated by the CalcuSyn Software (Biosoft, Cambridge, U.K.) for dose effect analysis (Effect) (Chou, T.C. and Talalay, P., Adv Enzyme Regul., vol. 22, p 27-55, 1984)

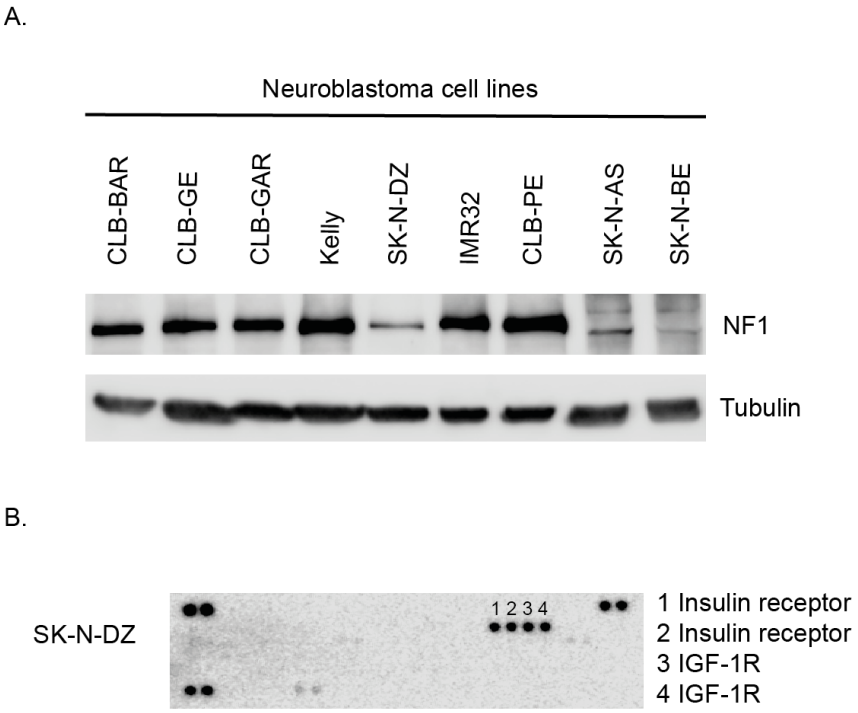

Figure S2: NF1 expression in neuroblastoma cell lines. (A) Immunoblotting for NF1 protein abundance in a panel of 9 neuroblastoma cell lines. (**B)** Phospho-RTK array blot from SK-N-DZ neuroblastoma cell lysates. Blots are representative of three different experiments.

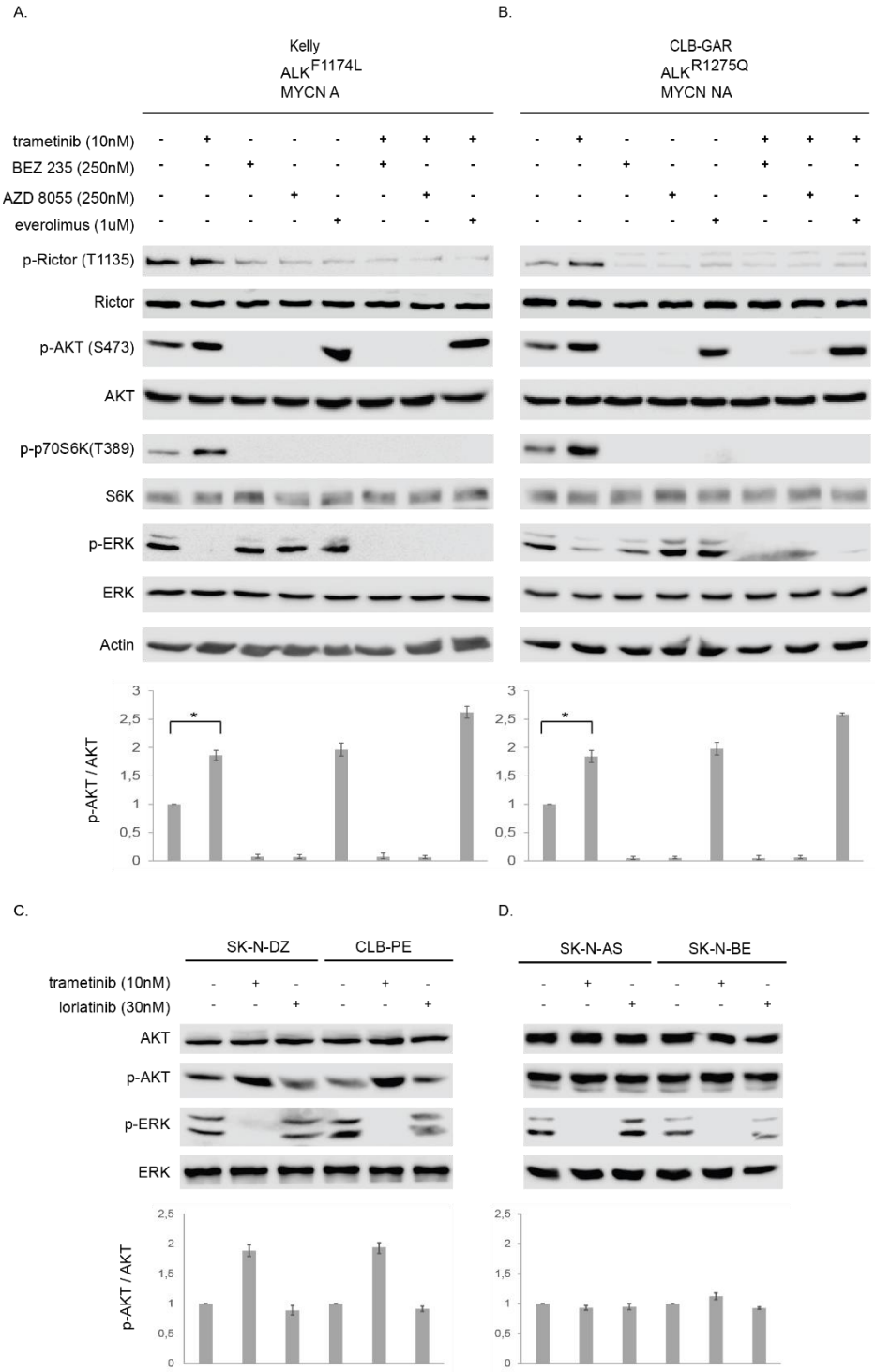

Figure S3: Sensitivity of neuroblastoma cell lines to trametinib. (A and B) Immunoblotting in lysates from ALK-positive neuroblastoma cell lines Kelly (A) and CLB-GAR (B) treated with trametinib, BEZ 235, AZD 8055, everolimus, or a combination as indicated. **(C and D)** TP53-mutant neuroblastoma cell lines SK-N-DZ and CLB-PE (C) and RAS-positive neuroblastoma cell lines SK-N-AS and SK-N-BE (D) treated with either lorlatinib or trametinib for 1 hour. Blots are representative; data are means ± SD of three different experiments. * $P <$ 0.002, Student's *t* test.

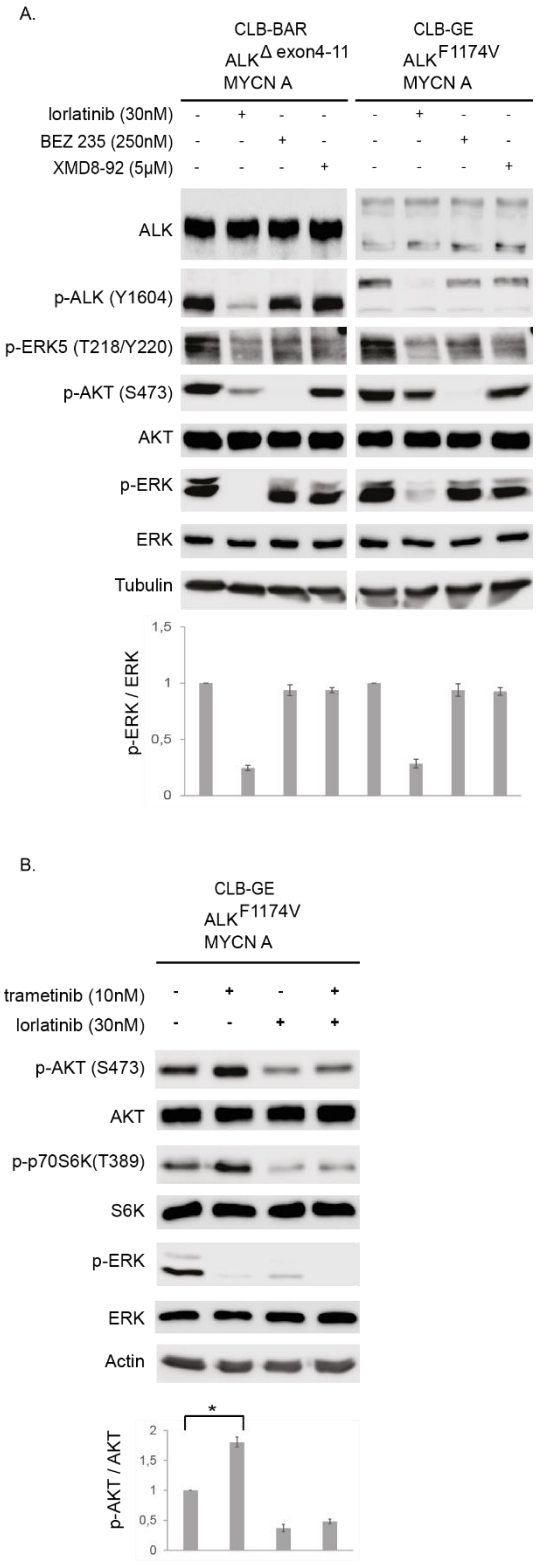

Figure S4: AKT signaling inhibition does not lead to increased activation of MAPK. (A) Immunoblotting in neuroblastoma cell lines CLB-BAR and CLB-GE treated with lorlatinib, BEZ 235 or XMD8-92 for 6 hours. **(B)** Immunoblotting in ALK-positive CLB-GE cells treated with trametinib, lorlatinib, or both as indicated. Blots are representative; data are means ± SD of three different experiments.

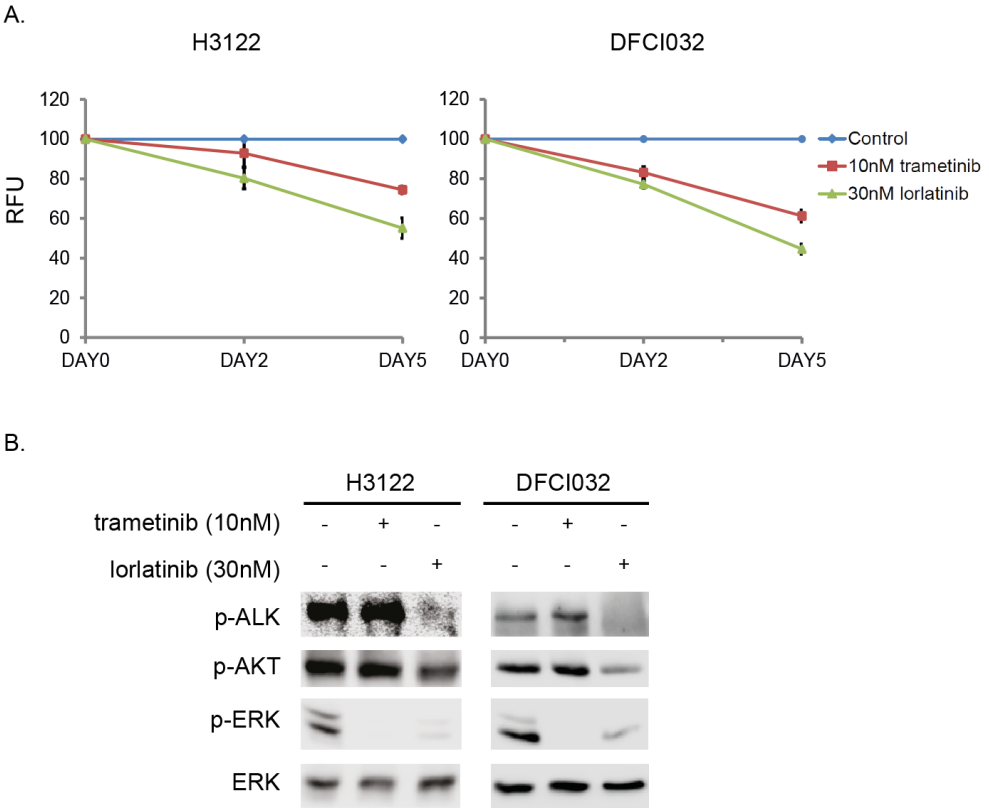

Figure S5. Sensitivity of EML4-ALK–positive NSCLC cell lines to trametinib. (**A**) Viability, assessed over 6 days with the resazurin assay, in EML4-ALK–positive NSCLC cell lines H3122 and DFCI032 treated with trametinib or lorlatinib as indicated.. Data are means of ± SE relative fluorescence units (treated cells relative to untreated cells) from three independent experiments. (**B**) Immunoblotting of whole cell lysates from cells described in (A) (p-AKT, Ser^{473}). Blots are representative of three experiments.

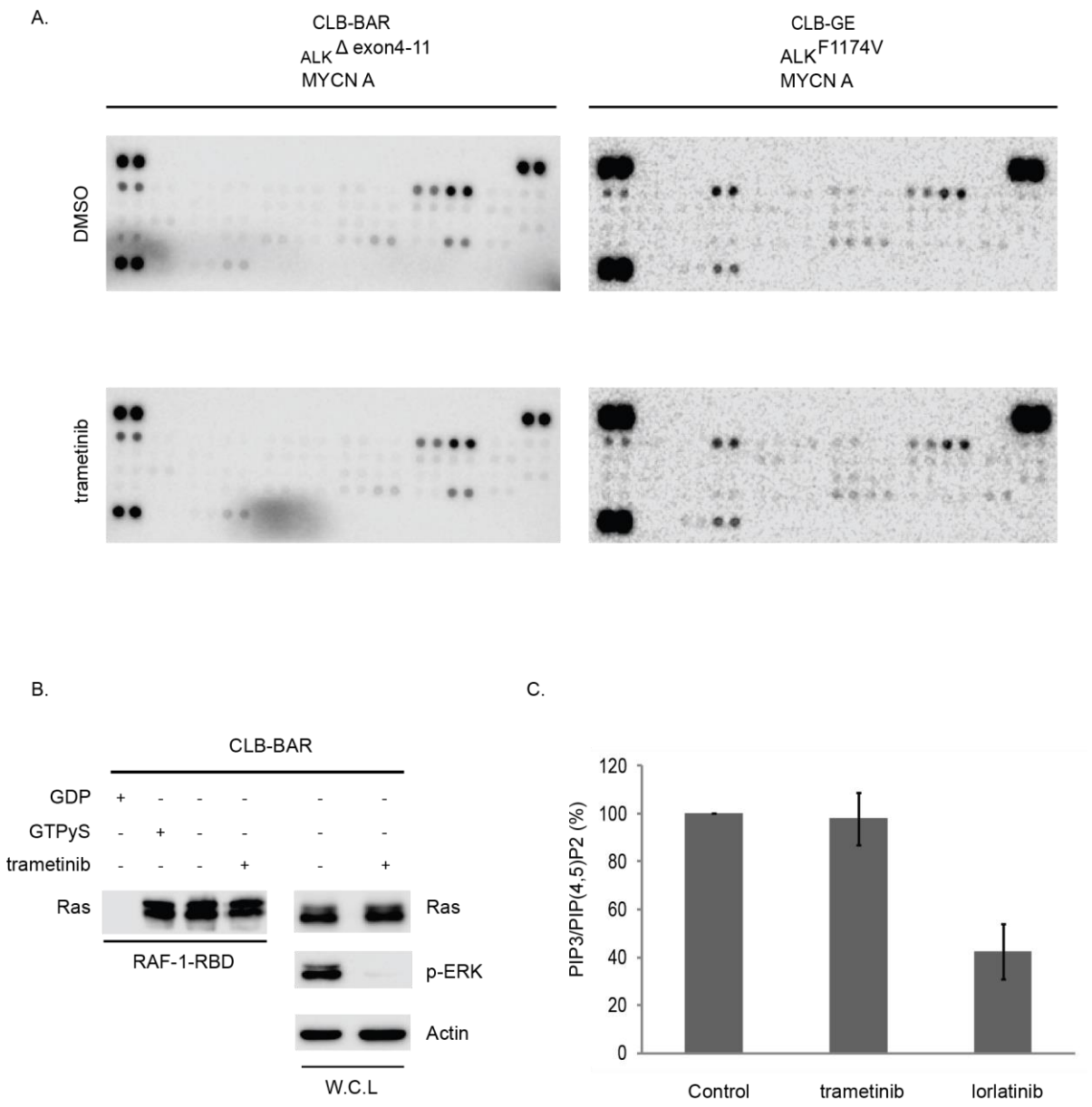

Figure S6: Phospho-RTK array analysis after MEK inhibition. (**A)** Phospho-RTK array recognizing 49 distinct RTKs incubated with lysates derived from ALK-positive neuroblastoma CLB-BAR and CLB-GE cells were treated with DMSO or trametinib (10nM) for 12 hours. (**B)** Immunoblotting for Ras in immunoprecipitates for active Ras (RAF-1-RBD, Ras-binding domain in RAF-1; left) from ALK-positive CLB-BAR cells treated with trametinib, GTPγS or GDP (to activate or inactivate Ras, respectively), or unperturbed. Whole cell lysates (W.C.L., right) were directly immunoblotted for Ras. (**C)** ELISA analysis for the amount of PIP3 relative to PI(4,5)P2 in phospholipid fractions isolated from CLB-BAR cells treated with either lorlatinib or trametinib as indicated. Blots are representative; data are mean ± SD of three independent experiments.

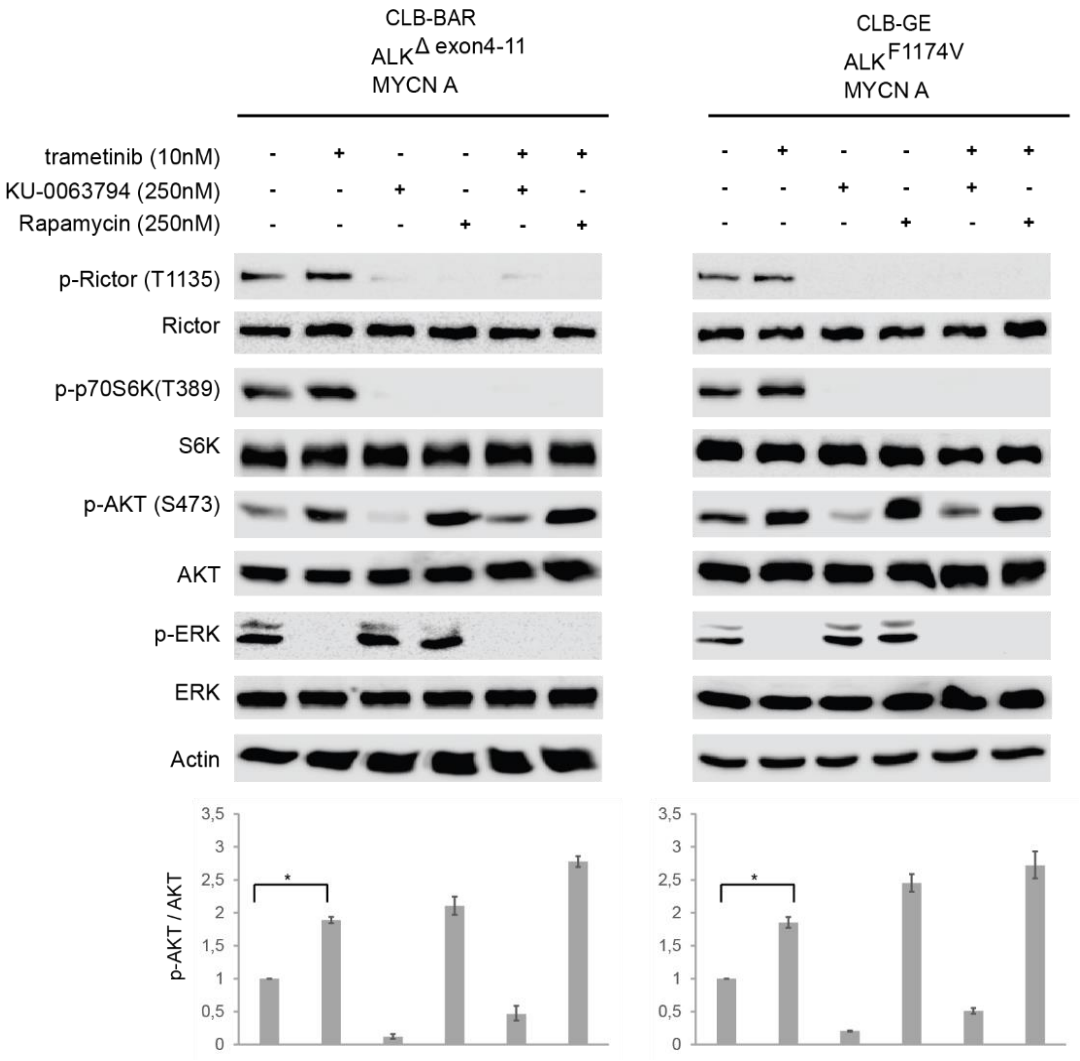

Figure S7. Increased AKT activation is observed upon treatment with trametinib and rapamycin. Immunoblotting of lysates from CLB-BAR and CLB-GE neuroblastoma cell lines treated with trametinib, KU-0063794, rapamycin or combination thereof as indicated. Blots are representative; data are mean ± SD of three different experiments. * $P < 0.006$, Student's *t* test.

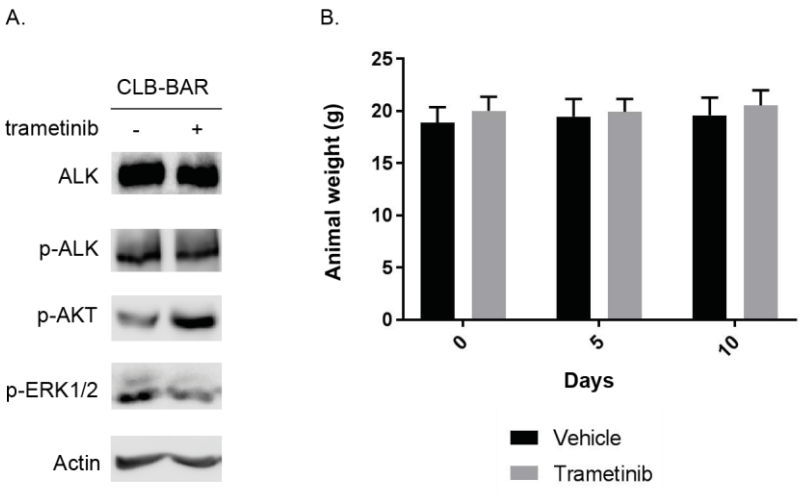

Figure S8: Increased activation of AKT upon treatment with trametinib. (A) Immunoblotting analysis of CLB-BAR xenografts in lysates from tumors collected after 11 days of treatment with either vehicle or trametinib. Actin served as the loading control. **(B)** Change in body weight relative to day 0 in mice receiving vehicle or trametinib (3mg/kg) over 10 days. No significant difference was detected between treatment and vehicle groups. Data are representative of three different experiments, n = 6 mice in each treatment group per experiment.

Cell line	Chromosomal rearrangements*	Genomic profile
CLB-BAR	Chr1:0(pter)-39,7/L; Chr2:9,3-9,5/A; Chr2:14,3-14,6/A; **Chr2:16-16,9/A; MNA** Chr2:20,8-21,1/A; Chr2:22,3-22,5/A; Chr2:29,3-29,816/A; Chr2:29,863-30,172/A; whole ALK except for part of intron 3 in amplicons* Chr2:32,1-32,2/A; Chr4:0(pter)-2/G; Chr6:100,1-171,1(qter)/L; Chr16:78,8-90,3(qter)/L; Chr17:36,9-81,1(qter)/G; Chr20:56,7-63(qter)/G;	MNA
CLB-GE	Chr1:0(pter)-17,2/L; Chr1:144,8-249,2(qter)/G; Chr2:2,4-3,3/A; Chr2:5,2-5,4/A; Chr2:9,9-10,2/A; Chr2:10,3-10,5/A; Chr2:10,6-10,7/A; Chr2:13,2-13,4/A; Chr2:13,5-13,6/A; **Chr2:16-16,4/A; MNA** Chr2:19,7-19,9/A; Chr2:29-30,1/; hela ALK amp Chr6:0(pter)-171,1(qter)/L; Chr7:85,6-159,1(qter)/G; Chr9:8,4-8,9/L; PTPRD del Chr9:111,3-113,6/G-; Chr10:42,6-135,5(qter)/L; Chr11:0(pter)-135(qter)/L; Chr16:0(pter)-32,4/L-; Chr16:32,4-90,3(qter)/G-; Chr17:46,6-81,1(qter)/G; Chr18:0(pter)-78(qter)/L; Chr22:0(pter)-51,3(qter)/G-;	MNA
CLB-GAR	Chr1:0(pter)-27,4/L; Chr2:0(pter)-29,9/G; break in ALK intron 1 Chr2:109,6-163,5/L-; Chr3:50,7-62,9/L-; Chr3:62,9-86,6/G; Chr4:0(pter)-25,2/L; Chr4:139,7-175/G; Chr4:175-191,4(qter)/L; Chr5:0-1,2/G; break in TERT intron 1 Chr5:149,5-180,9(qter)/L; Chr6:75,2-99,2/L; Chr8:40,2-41,3/G; Chr9:8,6-8,7/L; PTPRD deletion Chr11:0(pter)-41,2/G-; Chr11:41,2-44,5/L-; **Chr11:83,4-129,2/L; 11q-del** Chr12:72,6-133,8(qter)/G; Chr16:19,7-90,3(qter)/L; Chr17:0(pter)-8,1/G; Chr17:47-62,8/GG; Chr17:62,8-81,1(qter)/G; Chr20:45,6-63(qter)/G; ChrX:0(pter)-155,2(qter)/L; X,0	11q-del
Kelly	Chr1:0(pter)-3,4/G; Chr1:72,3-72,9/L; Chr1:97,7-249,2(qter)/G; Chr2:8,1-15,8/G; **Chr2:15,8-16,8/A; MNA** Chr2:16,8-43,7/G; Chr2:84,2-166,5/L; Chr3:29,5-29,9/L; deletion of RBMS3 Chr3:115,5-116,6/L; homozygous loss Chr3:118,5-198(qter)/G; Chr4:0(pter)-12,7/L; Chr4:181,8-183,6/L; Chr5:1,2-1,3/; possible TERT rearrangement Chr5:164,8-166,2/L; homozygous loss Chr6:162,3-162,7/L; homozygous loss in PARK2 Chr7:0(pter)-99,4/G; Chr7:99,4-115,6/L; Chr7:115,6-159,1(qter)/G; Chr9:9,4-9,7/; homozygot loss in PTPRD Chr9:68,6-123/L; Chr10:134-135,3/L; Chr11:0(pter)-22,1/L; **Chr11:114,7-135(qter)/L; 11q-del** Chr14:98-107,3(qter)/L; Chr16:6,2-6,8/L; homozygous loss in RBFOX Chr17:39,1-81,1(qter)/G; Chr18:0(pter)-15,1/L; Chr18:24-32,5/L; Chr18:34,9-35,8/L; Chr18:44,6-50,4/L; Chr18:50,4-50,7/L; homozygot loss in DCC Chr18:50,7-58,3/L; Chr18:68,2-69,6/L; Chr18:77,7-78(qter)/L; Chr20:50,4-63(qter)/G; Chr22:0(pter)-51,3(qter)/G; ChrX:0(pter)-98,6/L; ChrX:106,9-122,6/L; ChrX:127,6-155,2(qter)/L; XY	MNA + 11q-del
SK-N-DZ	Chr1:145-160/G; Chr1:162,7-249,2(qter)/L-; **Chr2:15,5-16,3/A; MNA** Chr2:0(pter)-243,1(qter)/Chrx; chromotripsis with at least 24 small loss regions Chr3:0(pter)-12,6/G; Chr3:36,3-81,1/L; Chr3:85-146,5/L-; Chr4:0(pter)-191,1(qter)/L; Chr8:101,6-146,3(qter)/L; Chr9:0(pter)-20,5/L; Chr9:20,5-29,5/LL; Chr9:85,7-109,9/L-; Chr10:0(pter)-12,5/G; Chr10:14-42,7/L-; Chr11:78,6-84,3/G; Chr11:88-95,5/G; Chr11:95,8-98,9/L; Chr11:102-134,9/L; Chr12:0(pter)-42,5/G-; Chr12:121-133,8(qter)/G-; Chr14:90,3-107,3(qter)/L; Chr16:6,4-6,8/L; deletion in RBFOX1 Chr16:7,1-7,7/L; deletion in RNFOX Chr16:71,9-90,3(qter)/G; Chr17:0(pter)-31,3/G-; Chr17:39,9-81,1(qter)/G-; Chr18:40,5-62/L-; Chr18:74,5-76,7/L-; Chr19:1,8-46,3/L-; Chr19:46,3-59,1(qter)/L; Chr20:29,8-63(qter)/G; Chr21:0(pter)-48,1(qter)/L-; ChrX:0(pter)-27,6/L; ChrX:29,3-155,2(qter)/L-; XX	MNA
CLB-PE	Chr1:0(pter)-148,5/G; Chr1:148,5-152,8/GG; Chr1:186,3-249,2(qter)/L; Chr2:0(pter)-14,9/G; Chr2:14,9-15,1/A; Chr2:15,1-15,3/G; **Chr2:15,3-16,6/A; MNA** Chr2:16,6-16,7/G; Chr2:16,7-17,5/A; Chr2:17,5-89,3/G; Chr2:149,9-243,1(qter)/G; Chr3:0(pter)-2,1/G; Chr3:15,8-83,9/L-; Chr3:86,3-98,3/L; Chr3:126,1-129,5/A; Chr4:52,8-70,2/G; Chr4:70,2-103,7/L; Chr4:103,7-191,1(qter)/G-; Chr5:0(pter)-138,1/G-; Chr5:146,3-180,9(qter)/L-; Chr6:0(pter)-110,5/G; Chr7:0(pter)-121,6/G; Chr7:138,1-159,1(qter)/G; Chr8:0(pter)-11,8/L; Chr8:11,8-146,3(qter)/L-; Chr9:8,4-8,4/L; Chr9:17,5-18/L; Chr9:25,7-72,8/L-; Chr9:72,8-141,2(qter)/G-; Chr10:0(pter)-53,8/L-; Chr11:0(pter)-55,8/L-; **Chr11:103,1-135(qter)/L-; 11q-del** Chr12:10,7-13,9/G; Chr15:0(pter)-102,5(qter)/G; Chr16:6,6-7,2/L; homozygous loss in RBFOX Chr16:87,8-90,3(qter)/L; Chr17:25,3-81,1(qter)/G-; Chr18:30,6-78(qter)/L-; Chr19:0(pter)-59,1(qter)/L-; Chr20:0(pter)-63(qter)/G-; ChrX:0(pter)-14,3/L; ChrX:113,6-155,2(qter)/L;	MNA + 11q-del
IMR32	Chr1:0(pter)-51/L; Chr1:51-249,2(qter)/G; **Chr2:14,7-16,1/A; MNA** Chr2:29,6-29,9/A; peak contains ALK ex 3-4 Chr2:53,3-53,6/A; Chr2:66,7-67,7/A; Chr2:69,1-69,4/A; Chr6:0(pter)-171,1(qter)/G; Chr7:0(pter)-57,5/G-; Chr12:0(pter)-133,8(qter)/G; Chr15:42,9-102,5(qter)/G; Chr16:69,9-90,3(qter)/L; Chr17:40,4-81,1(qter)/GG; XY	MNA
SK-N-AS	Chr1:1,8-11/L; Chr1:121,3-249,2(qter)/G; Chr3:0(pter)-60,6/L; Chr4:103,8-191,1(qter)/G; Chr6:108,9-171,1(qter)/L; Chr7:0(pter)-159,1(qter)/G-; Chr8:117,8-146,3(qter)/G; Chr9:0(pter)-23,7/L; Chr9:9,4-9,5/LL; homozygous loss in PTPRD Chr10:102,3-102,9/G; PAX2 **Chr11:71,5-135(qter)/L; 11q-del** Chr12:112-133,8(qter)/G; Chr16:83,4-90,3(qter)/L; Chr17:0(pter)-30,6/L; Chr17:40,9-81,1(qter)/G; Chr22:21,9-38,3/L-; Chr22:38,3-51,3(qter)/L; ChrX:0(pter)-155,2(qter)/L;	11q-del
SK-N-BE	Chr1:97-249,2(qter)/G; Chr2:0(pter)-1,9/L; Chr2:1,9-47,9/G; **Chr2:16-16,6/A; MNA** Chr2:190-243,1(qter)/G; Chr3:0(pter)-61,3/L; Chr5:96,7-98,6/G; Chr7:0(pter)-159,1(qter)/G-; Chr9:0(pter)-27,2/L; Chr9:126,6-141,2(qter)/G; Chr11:0(pter)-65,4/L; Chr11:65,4-135(qter)/G-; Chr12:0(pter)-111,5/G-; Chr13:0(pter)-85,3/L; Chr14:0(pter)-107,3(qter)/G-; Chr15:0(pter)-93,2/G-; Chr15:93,2-102,5(qter)/G; Chr16:5,7-5,8/L; Chr16:5,8-6,2/LL; homozygous loss in RBFOX1 Chr16:6,2-6,3/L; Chr17:31,2-81,1(qter)/G; Chr18:0(pter)-78(qter)/L; Chr20:0(pter)-3/L; Chr20:3-63(qter)/G-; Chr21:27,7-28,7/L; ChrX:0(pter)-155,2(qter)/L; X0	MNA

Table S1: Chromosomal profile of the cell lines. Chromosomal rearrangements identified in the nine neuroblastoma cell lines used in the study. The aberrations that define the genome profile are in bold letters. *Chromosomal rearrangements (chromosome, position in Mb fr pter, CRCh37/hg19, pter=aberration involve p-telomere pos=0, qter =aberration involve q-telomere, type of aberrations, aberrations of known significance in NB biology), L/G= loss/gain of one copy, L-/G- smaller relative loss(gain), LL/GG homozygous loss/extra gain of more copies, A=amplification.